EXPERIMENTAL INVESTIGATIONS OF STALL PROPAGATION IN AXIAL-FLOW COMPRESSORS

Thesis by

Toru Iura

In Partial Fulfillment of the Requirements

for the Degree of

Doctor of Philosophy

California Institute of Technology

Pasadena, California

1953

ACKNOWLEDGEMENTS

The author wishes to express his gratitude to Professor W. Duncan Rannie for his inspiration and guidance in conducting these experiments and to Professor Frank E. Marble for many stimulating discussions concerning the propagating stall. Special thanks are due to Mr. F. T. Linton for his aid in the experiments.

ABSTRACT

Hot-wire anemometer measurements of the velocity fluctuations in stalled operation of an axial-flow compressor have demonstrated that stalling occurs as more or less well-defined regions of retarded flow which rotate in the compressor annulus without changing shape. These regions propagate in the direction of the blade rotation with a speed proportional to, but of smaller magnitude than, the rotor speed. Two principal types of propagating stall were observed. The one with the stalled region or regions extending over part of the blade height was defined as partial stall, and the other with a single stalled region over the entire blade height was defined as full stall.

TABLE OF CONTENTS

I. SUMMARY

The importance of understanding the behavior of an axial-flow compressor in stalled operation has become extremely vital to the further development of modern turbojet engines. The possibility of compressor stall occurring during starting and accelerating operations of turbojet engines has increased with the use of progressively higher design compressor pressure ratios required for greater engine efficiencies. This condition is undesirable because of the resultant low efficiencies and also because of the possibility of blade failure due to vibrations induced by the phenomenon.

Although it is evident that compressor stall occurs from the stalling of blades in its individual stages, the manner in which this occurred was not known until recently. Most of the past work has dealt with the phenomenon of compressor surge, where the flow rate averaged over the compressor annulus fluctuates with time. The stable limit of compressor operation has been termed alternatively the surge line or stall line without any clear cut distinction between the two. Previously, stalling of the blades was thought to occur symmetrically with the same portions of all the blades in a blade row stalled simultaneously.

Experiments were conducted on a large, low speed axial-flow compressor with one stage of "solid body" and

"free vortex" blading and also with three stages of "free vortex" blading. Velocity fluctuation measurements have demonstrated that stalling in an axial-flow compressor occurs as asymmetric regions of separated or retarded flow which rotate unchanged in shape about the compressor axis. The regions of retarded flow are usually well-defined and are propagated circumferentially with a velocity proportional to, but of smaller magnitude, than the rotor speed. This new phenomenon will be defined as propagating stall and here, in contrast with surge, the flow rate averaged over the annulus is constant.

Qualitatively, propagating stall can be pictured as a successive stalling and unstalling of blades in an infinite cascade with the stalled region, which may cover several blade channels, propagating along the blade row. In a compressor, this corresponds to a well-defined region of retarded flow rotating about the compressor axis. Two principal types of propagating stall were observed; these are defined as "Partial Stall" and "Full Stall". Partial stall was characterized by one or more well-defined stall regions extending over a portion of the blade height, with the stalled region concentrated either at the blade root or tip. Full stall was characterized by a single rotating region of retarded flow extending over the full blade height and propagating at a speed lower than that for partial stall. Hot-wire anemometers were used to determine the extent, number, and rotational speed of the regions of

retarded flow.

The investigations described here are concerned primarily with the propagating stall, which probably occur in all axial-flow compressors as they are throttled beyond the peak pressure point. No distinct surge was observed although it may have existed in some of the compressor configurations studied. Surging possibly involves an oscillation from one propagating stall pattern to another, the frequency of the surge being determined by the characteristics of the ducting or reservoirs in the compressor circuit.

Theoretical investigations of stall propagation in two-dimensional cascades have been made by Sears and Marble, and these have shown the possibility of propagating disturbances under certain assumptions of phase lag between the fluctuating lift and mean angle of attack of the blades, or of non-linear blade characteristics. The characteristic time associated with the stall propagation could not be determined from these theories. Previously, it was believed that the characteristic time is connected with the time required for establishment of a separated boundary layer when an airfoil of a cascade is subjected to a sudden change of angle of attack. The experiments described here indicate that this time is relatively independent of the number of blades and of the detailed nature of the flow through the blades. Hence the earlier picture

of the mechanism governing the characteristic time has been discarded.

II. INTRODUCTION

An important problem facing the designer of aircraft axial-flow compressors today is that of compressor stall. The mechanism of compressor stall must be understood and means of anticipating and alleviating it must be found in order to improve the off-design performance range of modern high-pressure-ratio compressors.

Stable operation of an axial-flow compressor is not usually possible over its entire flow range from maximum flow to shut-off. For example, when the flow rate is reduced, say, at constant rotor speed, a point will be reached at which the flow pattern becomes very unstable. This instability of flow is characterized by periodic fluctuations of flow in the compressor, and is often accompanied by severe noise. Turbojet operation in this region is undesirable, not only from the standpoint of resultant low efficiencies, but also from the standpoint of possible structural failure due to vibrations induced by the phenomenon.

Investigations in the past (Ref. 1, 2, 3) have been concerned primarily with the phenomenon of compressor surge, where the flow rate averaged over the compressor annulus varies with time. The stable limit of compressor operation has been termed alternatively the surge line or stall line without any clear cut distinction between the

two. Previously, stalling of the blades was thought to occur in a symmetric fashion, with the same portions of all of the blades stalled simultaneously. However, the experiments to be described in this thesis have demonstrated that stalling in axial-flow compressors occurs as asymmetric regions of separated or retarded flow which rotate unchanged in shape about the compressor axis. This new phenomenon will be defined as propagating stall, and here, in contrast with surge, the flow rate averaged over the compressor annulus is constant. However, before describing the propagating stall in detail, the importance of the compressor stall problem as applied to aircraft turbojet units will be discussed.

The possibility of compressor stall occurring during the starting and accelerating operations of a turbojet engine has increased with the use of progressively higher design compressor pressure ratios required for higher engine efficiencies. This may be demonstrated by considering a performance map for a conventional axial-flow compressor, where a family of curves of pressure ratio versus flow rate are plotted for various values of the rotor speed.

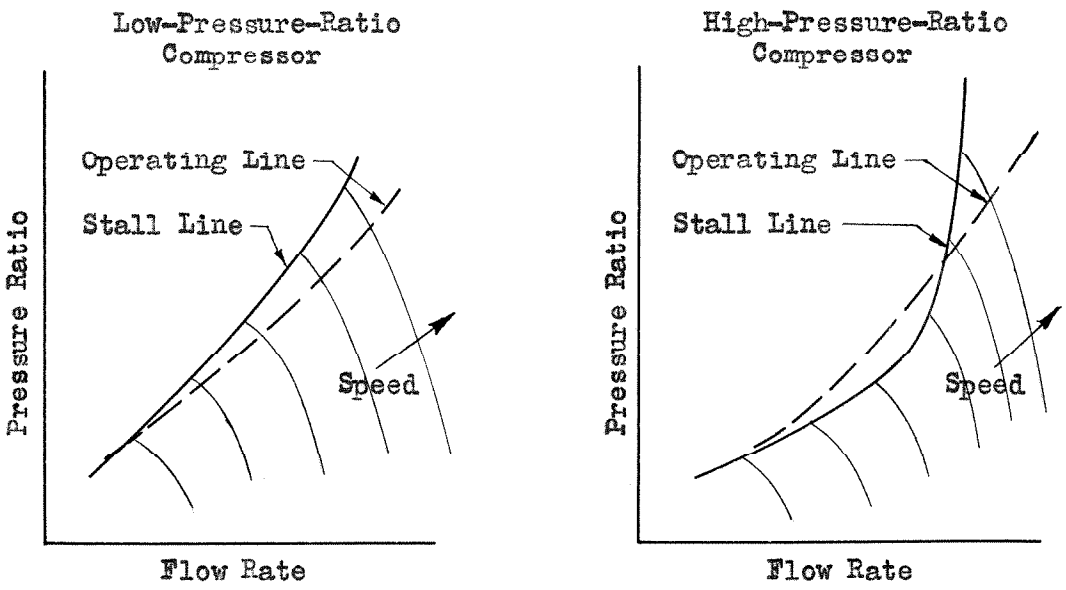

Fig. 1a: Sketch of Performance Maps for Axial-Flow Compressors.

The stall line is the locus of points on the pressure ratio curves at which marked instability occurs, usually a line through the peak pressures. For a compressor of low pressure ratio, the operating line (which is determined by the turbine characteristics and the combustion chamber temperatures) lies within the stable operating range of the compressor for all except the lowest rotor speeds, therefore, the compressor unstalls at relatively low speeds in a starting operation. For a compressor with high pressure ratio, the stall line usually has a sharp bend as shown in the sketch above, so that it intersects the operating line at higher rotative speeds. Hence when starting the turbojet engine up to design speed, the compressor may be stalled until very high rotor speeds, causing it to possibly cease operating or

induce vibrations serious enough to damage the compressor blades.

In a turbojet engine, it is necessary to match the turbine power output to the compressor power requirements, hence when accelerating the engine, greater turbine torque is required resulting in higher turbine temperatures. This requires a higher compressor pressure ratio to push the gases through the turbine, bringing the operating line nearer or even into the stall regime. To allow satisfactory accelerating properties, the turbine nozzle area may be increased or another stage added to the high pressure end of the compressor to distribute the load in the stages. Although either of these methods would tend to alleviate the possibility of stall and still allow a turbine temperature to give the required rate of acceleration, they are used at a sacrifice in efficiency and therefore are not practical if the loss in compressor efficiency incurred by avoiding stall exceeds the gain obtained from the additional stage.

Another innovation for allowing high-pressure-ratio performance is the twin-spool engine. In this design, the compressor is divided into two sections capable of independent rotational speeds. As a consequence, the differing speeds of the two units will allow more favorable geometric flow angles over a wide range of operating speeds than with a single spool with the same pressure ratio.

It is evident that compressor stall arises from the stalling of its individual stages, and the manner in which this occurs is dependent on operating conditions. An axial-flow compressor is usually designed so that the individual stages are matched to keep the axial velocities uniform or nearly so in all stages, i.e, its annular area decreases progressively to conform to the increasing air density towards the discharge end at design speed. When the engine is starting or operating at very low speeds, the compression ratio is quite low, causing the density variation of the air to be different from design. This leads to low axial velocities in the first stages and correspondingly high velocities in the exit stages. As a result, the compressor will stall at low rotational speeds due to stalling of the inlet stages. This condition becomes more acute with higher design pressure ratios.

At higher than design speed, the last stages will tend to stall and the first stages to unload. This is caused by the density ratio being higher than design, which leads to lower axial velocities and possibly stalling conditions in the exit stages.

As was mentioned earlier in this section, the concept of stalling has changed with recent developments. This thesis gives the results of experimental investigations of stalling in a large, low speed axial-flow compressor, which show that stalling occurs as regions of separated

or retarded flow which are not axially symmetric, but occur in more or less well-defined areas around the circumference of the compressor annulus. The regions of retarded flow remain approximately the same shape and are propagated circumferentially with a velocity proportional to the rotor speed. This phenomenon will be called propagating stall, and it is characterized by the flow rate averaged over the compressor annulus being constant. Surging will be defined as a phenomenon where in contrast to stall, the flow rate averaged over the compressor annulus fluctuates with time. Surging possibly involves an oscillation from one propagating stall pattern to another, the frequency of the surge being determined by the natural frequency of the ducting or reservoirs in the compressor circuit. Although the propagating stall phenomena have been mentioned by other investigators, the only paper reporting measurements is one given recently by Huppert and Benser (Ref. 4).

The investigations described in this thesis are concerned principally with stall propagation. No distinct surge was observed although it may have been existent in some of the compressor configurations studied. It is believed that probably more or less well-defined stall propagation phenomena occur in all axial-flow compressors as they are throttled beyond the peak pressure point. Similar phenomena have been observed in centrifugal

impellers and even in straight cascades by Dr. H. Emmons (private communication to Prof. Rannie). Propagating stall cannot be detected by pressure or velocity measurements with instruments of low response time, and it is necessary to resort to hot-wire anemometers or high frequency pressure pick-ups for detection of the phenomena.

Propagating stall has been explained qualitatively as a successive unstalling and stalling of blades in a cascade. The stalled blade channels offer a high resistance to flow through the cascade and the approaching flow tends to be diverted to each side of the stalled region as shown in Fig. 1. The incidence angle is reduced to the left of the stalled blades and increased to the right. This tends to stall the next blade on the right and unstall the last stalled blades on the left. The stalled region hence moves to the right. Apparently, as the average flow angle of a cascade approaches stalling incidence, the preferred flow pattern is one with groups of blades severely stalled alternating with groups of unstalled blades rather than a uniform stalling of all blades. The velocity of propagation is determined by some characteristic time, the origin of which is not definitely understood at present. For a moving cascade, the stall propagation speed relative to a fixed system is the difference between the cascade speed and the propagation

speed in the moving cascade. All propagating stall patterns observed moved relative to the compressor casing in the direction of the rotor with a speed less than the rotor speed (Fig. 2).

III. TEST EQUIPMENT

3:1 Test Compressor and Instrumentation

The compressor used in the stall propagation measurements was one designed to simulate internal flow patterns commonly employed in modern high performance turbomachines. A cross section of the test installation is shown in Fig. 3 where the principal dimensions are also summarized. The air flowed into the compressor through a cylindrical entrance duct with a bell mouth opening. A screen was installed on the bell mouth to prevent foreign objects from entering the compressor air stream. An interconnected set of four wall static pressure orifices was located midway through the entrance duct, which was calibrated to give the total air flow rate or flow coefficient. After acquiring an initial circumferential component from a set of pre-rotation vanes, the air flowed through successive rotating and fixed compressor blades as shown in Fig. 3. The exit portion of the installation consisted of a short cylindrical duct, an elbow section, and a transition section which connected the elbow to the throttle valve. The throttle valve which regulated the flow resistance and thus the compressor flow volume, consisted of two rectangular metal doors which could be actuated by a variable speed motor to vary the throttle opening and hence the flow rate.

A 125 H.P. electric dynamometer drove the compressor by means of a shaft which passed through the rear duct. The power input to the compressor could be found from accurate measurements of the rotative speed and of the driving torque which was determined by means of a diaphragm type force meter manufactured by the Hagan Corporation (see Ref. 5).

The compressor was constructed so that each blade was separately removable, hence a variety of blade and stage configurations were possible. Two types of blades were available, three stages of "free vortex" blading and one stage of "solid body" blading. Both sets were designed for an average power coefficient $\bar{\Psi} = 0.40$ at a flow coefficient $\bar{\Phi} = 0.45$. The design power coefficient was actually attained at $\bar{\Phi} = 0.43$ because of the influence of the wall boundary layers. The compressor blade tip diameter was 36 inches and the hub ratio 0.6. The blade solidity ranged from a maximum of 1.150 at the rotor roots for both types to a minimum of 0.690 for the free vortex rotor tip and 0.903 for the solid body rotor tip. The blade sets are shown in Fig. 4, and the geometric properties are summarized in Table 1. There were 30 rotor blades and 32 stator blades in respective rows. The axial spacing between the center lines of adjacent blade rows was 2.875 inches. Most of the measurements

were made at a compressor rotative speed of 750 rpm (u_o = 118 fps), hence compressibility effects were negligible, and the blades could be considered rigid as far as aerodynamic forces were concerned.

The entrance duct had a volume of 51 cu. ft. and the exit duct (between the compressor and the throttle), a volume of about 46 cu. ft. The calculated natural frequencies of the system considered as a Helmholtz resonator were above 22 cps except one mode involving coupling between the air volume and the drive shaft assembly, which was estimated as 18 cps. All propagating stall patterns, with one exception, had frequencies lower than the above. This one exception represented a metastable stall pattern which quickly reverted to one of lower frequency.

Instrument surveys downstream of each rotor and stator row were possible through the provision of six rectangular instrument ports located near the top of the outer case and a set of radial survey holes provided at several circumferential positions behind each blade row. A traversing carriage, described in Ref. 5, was used to position the instrument probe in the compressor ports; and a radial survey carriage, illustrated in Fig. 5, was used to position the probes in the radial survey holes.

The flow rate through the compressor was determined by measurements of velocity profiles which were corre-

lated with the entrance duct wall static pressure. With a calibration chart of wall pressure vs. discharge rate, it was then possible to determine the flow rate by reading the wall pressure. The wall static pressure was measured with a water-micromanometer manufactured by the Meriam Instrument Company. This instrument, which is of the "movable well type", can be read to an accuracy of 0.001 inch of water.

Measurements of the exit-duct wall static pressure were made simultaneously with the torque measurements to obtain a quickly available idea of the pressure rise in the compressor. These pressures were measured with an electric pressure transducer manufactured by the Statham Company, Los Angeles, California. The pressure detecting unit which consisted of a bridge circuit and a Brown "Electronik" precision indicator is shown at the right in Fig. 6 and described in detail in Ref. 6.

The foregoing information describes the salient features of the compressor installation as used for the stall propagation experiments. Further details may be obtained from Ref. 5 and 6.

3:2 Hot-Wire Equipment

For velocity fluctuation measurements, radial hot-wire anemometers utilizing platinum wires of 0.00024 in. diameter and 3/16 - in. length were employed. The hot-

wire probe and its radial positioning carriage are shown in Fig. 5. The wires were manufactured by the Wollaston process, therefore were supplied with a silver jacket which was used to protect them during the manufacturer's drawing down process. Before using the wire, it was necessary to remove the outer jacket by immersing it in a nitric acid solution. The platinum wire was soft soldered to the supports and results indicated that it was sufficient to give a good mechanical and electrical bond.

A general view of the hot-wire instruments is shown in Fig. 6, and a schematic diagram of the apparatus is shown in Fig. 7. The hot-wire heating circuit and amplifier were designed and constructed by the Thiele-Wright-Rothbart Co. of Los Angeles, California. In the majority of the tests, a constant current of 50 milliamperes from a 90-volt B battery was used. The use of a relatively large battery source was to keep the current as nearly constant as possible, and this was found sufficient to limit current fluctuations to less than one percent even with large velocity changes.

The hot-wires were calibrated in the entrance duct of the compressor by finding values of its resistance under constant current conditions at several known values of air velocity. By plotting R/R-Ra against $\sqrt{v}$, a straight line relationship was obtained, necessitating only a few points for the calibration (Fig. 8). This

relationship is the conventional King's equation for the wire normal to the air stream:

$$i^2 \alpha R_o \frac{R}{R - R_a} = a + b\sqrt{V}$$

The calibrations were made before and after each test run, and from the linear relationship obtained, a second curve of resistance (R) vs. air velocity (V) was plotted (Fig. 9), which was used to determine the velocity values under test conditions.

For phase measurements, two identical circuits were used so that simultaneous readings with two separate hot-wire probes could be made. The two circuits were checked for identity in response time so that phase measurements for the determination of the number of stalled regions could be made with two probes in different circumferential positions. This was done by feeding a common oscillator signal into both channels and checking the Lissajous figures created by the two output signals on an oscilloscope.

For the preliminary study of stall propagation, it was found convenient to use a direct-inking type oscillograph manufactured by the Brush Electronic Co., Cleveland, Ohio (Model BL-202). This, together with a Brush BL-905 amplifier had the advantage of making instantaneous, permanent chart records although the frequency response of the unit was flat only up to 100 cycles per second (see

Fig. 10). This limited the response of the entire unit since the hot-wire amplifier had a flat frequency response up to about 1000 cycles per second as shown in Fig. 11. However, this response was felt to be adequate for the investigation of the observed pulsations ranging from 1.5 to 15 cycles per second.

The over-all calibration of the amplifier system was found by introducing known resistance changes (by means of a vibrating contactor) in the hot-wire line under actual operating conditions, and correlating this with the square wave signals produced on the oscillograph. The results of various calibrations for a given amplifier gain setting are shown in Fig. 12, where the peak input voltage to the oscillograph unit is plotted as a function of hot-wire resistance change. The oscillograph unit was provided with a calibration device which permitted any pen deflection to be translated in terms of input voltage. This, together with the hot-wire velocity response, provided the necessary information to interpret the oscillograph signals in terms of velocity fluctuations. Because of the low frequency response of the unit, it was not possible to record individual rotor wakes.

IV. COMPRESSOR STALL WITH THREE-STAGE FREE VORTEX BLADING

4:1 Introduction

The experimental results obtained from the compressor with three stages of free-vortex blading will be discussed first, because this configuration produced the most clear cut examples of the various types of stall propagation observed. The regions of stall for this configuration are shown in Fig. 13a and b, which are plots of torque and exit-duct wall pressure as functions of flow coefficient at a compressor rotative speed of 750 rpm. It will be noted that the first signs of stall on closing the throttle occur in the form designated as "partial stall" at a flow coefficient slightly lower than the maximum torque and exit-duct pressure points. The region of partial stall extended to a flow coefficient slightly above $\bar{\Phi} = 0.30$, where the exit-duct wall pressure dropped off suddenly, and the compressor went into a regime designated as "full stall". The exit-duct wall pressure did not change appreciably in the full stall region. On closing the throttle, the compressor went into both partial and full stall at lower flow coefficients than when the flow rate was being increased at constant rotor speed. There was a definite hysteresis loop in the transitions between partial and full stalls. In terms of audible noise, partial stall was detectable by a rumbling noise that was

slightly louder than the normal operating noise, and full stall was perceptible by a rumbling sound of very distinct periodicity.

4:2 Partial Stall

When the term "partial stall" is used, it is in the sense that only a part of the radial extent of the blade is experiencing stall. Hot-wire anemometer measurements showed periodic velocity fluctuations only in the region of the blades extending from the hub to about mid-radius. (Partial stall in the blade tip region was observed with other compressor blade configurations, as will be discussed later.) Initially, as the flow was throttled (at 750 rpm or 12.5 rps), the hub region disturbance had an average frequency of about 4.7 cycles per second. This disturbance extended to about mid-radius, and further throttling did not cause any appreciable change in the magnitudes of the velocity fluctuations. However, the observed frequency increased to about 9.4 cycles per second, and on further throttling, became 14.1 cycles per second. Fig. 14 shows examples of the chart data obtained with the oscillograph. The principal types of partial stall patterns are shown as they appear with two different chart speeds of 25 mm per sec. and 125 mm per sec. The one-region partial stall fluctuations are shown at three different radii, and it can be seen that the fluctuations disappear entirely at mid-radius. The magni-

tudes of the instantaneous velocities, as measured, show strongly retarded flow regions that can result only from flow separation (stalling) on the blades. The mean velocity $\bar{V}$ is the average of the instantaneous velocities with respect to time over a complete cycle as determined by the mean resistance of the hot-wire. For velocity fluctuations large compared with the mean velocity, this procedure introduces some error. The portions of the velocity traces above the chart center line in general correspond to unretarded flow, while those below correspond to retarded flow. The amplitude of the velocity fluctuation ΔV was taken as the difference of the minimum velocities in the unretarded and retarded flow regions. The radial distribution of the velocity fluctuation amplitude ratios, $\Delta V/\bar{V}$, are shown in Fig. 15

Two hot-wire anemometers were inserted to the same radii in a plane normal to the compressor axis as shown in Fig. 16 and their angular separation varied. The phase difference of the velocity patterns as measured with the two probes was equal to their angular separation for the fluctuations with frequency 4.7 cps, equal to twice the angular separation for the fluctuations with frequency 9.4 cps and three times the angular separation at 14.1 cps (see Fig. 17). The probe displaced in the direction of rotation lagged behind the other probe in all cases. It is clear from these observations that the

three frequencies represent respectively one, two, and three propagating stall regions uniformly spaced around the circumference (Fig. 18).

Since the rotor speed was 12.5 rps in these tests, the partial stall regions rotated with 38 percent of the rotor speed in the direction of the rotor motion. Each of the three stalled patterns above was very stable in a narrow throttle range. The single pattern occurred in a very narrow flow coefficient range of about $0.40 > \bar{\Phi} > 0.39$ for closing throttle. The maximum width of the single region of retarded flow was about 17 percent of the circumference, which corresponds to approximately 5 rotor blade channel widths. At a flow coefficient $\bar{\Phi} \cong 0.39$ the single stalled region became unstable and split into two regions which oscillated in their relative positions, but with further slight throttling, the two regions separated and finally took up stable positions 180 degrees apart. In this condition, the two regions were of nearly equal size and had the same maximum width, about 5 rotor blade channel widths. They did not differ significantly from the single region at the higher flow rate. The two-region partial stall was the stable pattern for the range of approximately $0.39 > \bar{\Phi} > 0.37$. At $\bar{\Phi} \cong 0.37$ the two-region pattern became unstable, a further splitting and rearrangement occurred, and on very slight throttling, a three-region pattern of retarded flow became the stable

pattern. The maximum width of each of the three regions, which were 120 degrees apart, corresponded to about 4 rotor blade channel widths (Fig. 18). The radial extent of each of the regions increased slightly with closing throttle, however, the maximum velocity fluctuation ratio at the hub was about the same ($\Delta V/\overline{V} \cong 0.65$) for all three types (Fig. 15). On closing the throttle to a flow coefficient $\overline{\Phi} \cong 0.30$ the three-region pattern became unstable and full stall (described later) appeared.

When the throttle was opened from the full stall point, the above patterns appeared in reverse order, although the limits of ranges of succeeding patterns occurred at larger flow rates than on closing throttle. The three-region pattern appeared at $\overline{\Phi} \cong 0.34$ and the one-region pattern disappeared at $\overline{\Phi} \cong 0.41$. In one instance, four symmetrical propagating stall regions appeared on opening the throttle from the full stall. Although well-defined, the pattern was soon replaced by the three-region pattern without touching the throttle (see Fig. 14).

The blades tended to stall near the hub first as the throttle was closed. Apparently an alternating pattern of stall is more stable than an axially symmetric stall. The strong retardation of the flow in the stalled region causes an increased flow rate and hence an unstalling tendency over the remainder of the annulus. It might be thought that further throttling would simply increase the

size of the stalled region. However, the circumferential pressure distribution behind the stalled blade row must be controlled largely by the unstalled axially symmetric flow beyond the mid-radius, and this, one would expect to be nearly uniform around the circumference. Unrestricted growth of the single partial stalled region would lead to a strong asymmetry incompatible with the symmetry of the flow beyond mid-radius. Hence, the increased area of the region of stall appeared as two equal regions symmetrically placed as if in an effort to keep the pressure as uniform as possible. Further throttling caused three symmetrically placed patterns to appear for similar reasons. Evidently, a completely axially symmetric stall is unstable compared with the alternating stalled regions and the minimum width for a single stalled region corresponds to 4 or 5 rotor blade channels. As long as the outer portion of the annulus is unstalled, the area of the single stalled region cannot grow indefinitely, but multiple patterns of the minimum area stalled region can arise, tending to keep the over-all flow and in particular the pressure as symmetrical as possible. The stalled regions were very sharply defined and demonstrated characteristics of certain types of nonlinear oscillations. A given throttle setting allowed two alternative patterns and very slight disturbances caused one or the other to appear. Closing or opening the throttle a small amount eliminated one or the

other completely.

4:3 Full Stall

As the compressor was throttled, a sharp transition occurred at a flow coefficient of $\bar{\Phi} \simeq 0.30$ from partial stall to full stall. Full stall is characterized by a propagating stall region that extends over the entire blade height. The average exit-duct pressure showed no significant change from this point to complete shut-off while the torque continued to decrease slightly and then increased uniformly to shut-off. The propagating speed of the full stall did not change significantly, ranging from 26 percent of the rotor speed at the initiation of full stall to 30 percent of the rotor speed at shut-off. At any given flow coefficient in the full stall region, the propagating speed was the same whether the flow rate was reached by opening the throttle or closing the throttle (see Fig. 19).

The extent of the region of retarded flow in full stall at a flow coefficient $\bar{\Phi} = 0.323$ (opening throttle) is shown in Fig. 20 and 21. The region is widest at the hub where it occupies about 12 rotor blade channel widths and its width decreases toward the tip where it occupies 2 rotor blade channel widths. The growth of the retarded flow region at mid-blade height as the flow coefficient is decreased is traced in Fig. 22. The width of the stall region increases from about 7 rotor blade channel widths

at the beginning of full stall to almost 26 channel widths at shut-off. Fig. 23 shows sample oscillograph records of velocity fluctuations in the full stall regime. It will be noted that the retarded flow region is characterized by irregular velocity fluctuations.

The magnitudes of the velocity fluctuations in full stall were nearly constant over the entire blade length ($\Delta V/\overline{V} \cong 0.7$) as contrasted with the situation in partial stall, where the velocity fluctuations decreased in magnitude radially from the hub (Fig. 15). The velocity fluctuations in full stall at mid-blade height behind the first and the third rotors are compared in Fig. 24. The magnitude of the peak velocity fluctuation amplitude ratio, $\Delta V/\overline{V}$, was larger behind the third rotor than behind the first rotor indicating a more severe disturbance in the rear stages. Undoubtedly reverse flow occurred in the full stall regime, particularly at low flow rates. The hot-wire records do not show this clearly since velocity magnitudes alone were measured. Visual observations of cotton tufts inserted in the compressor air stream showed the presence of reversed flow at low over-all flow rates, mostly toward the hub.

An investigation of the influence of the volume of ducting was made in early tests. Blocking off the rear of the compressor annulus increased the full stall propagating velocity from 30 percent of the rotor speed to about

40 percent. Blocking off both front and rear of the compressor annulus so as to eliminate all effects of ducting resulted in a propagation velocity of about 45 percent of the rotor speed. Although these drastic restrictions have some influence, it is evident that the propagating stall is primarily a characteristic of the blading and its occurrence is independent of the presence of ducts.

If surging occurred, the frequency would be expected to be high, that is 20 or 30 cps, corresponding to the resonator frequencies of the ducting and much higher than the frequencies of passage of the propagating stall at the rotor speeds used. No surging was recognized in any of the flow regimes above, although there is a possibility that surging occurred in some of the configurations discussed later.

4:4 Effect of Removing the Third Stator Row

Upon removing the blades of the third stator row, that is the last row of the three-stage free vortex blading, the most significant effect was that no multiple partial stall patterns occurred. A single rather unstable partial stall appeared at the hub at a flow coefficient $\bar{\Phi} \cong 0.38$ on closing the throttle. This flow coefficient was smaller than that marking the beginning of partial stall with the third stator in place. Full stall commenced at $\bar{\Phi} \cong 0.36$, a higher flow coefficient

than with the third stator. The propagation velocity of both partial and full stall regimes were nearly equal and both slightly greater than the full stall velocity with the third stator (Fig. 19). Similar to the case with the third stator in place, partial stall occurred at a flow coefficient slightly lower than the maximum exit-duct pressure point, however, the exit-duct pressure decreased at a greater rate with closing throttle until the full stall point, where it dropped off suddenly. The exit-duct wall pressure also showed a hysteresis effect at the transition points between partial and full stalls.

4:5 Effect of Solidity

By removing alternate blades from each blade row in the three-stage free vortex compressor, it was possible to observe the effect of a change in solidity on the stall propagation. Partial stall of the multiple type was not found although a region of small irregular velocity fluctuations was observed on throttling at a flow coefficient $\bar{\Phi} \cong 0.35$. The variation of propagating stall speed with flow coefficient is shown in Fig. 25. Full stall commenced at $\bar{\Phi} \cong 0.33$ with one stalled region propagating in the direction of compressor rotation at 27 percent of the rotor speed. The propagation speed decreased with throttling until $\bar{\Phi} \cong 0.29$, from which point it remained constant at slightly under 20 percent

of the rotor speed. At $\bar{\Phi} \cong 0.07$, the one-region propagating full stall deteriorated into a rather irregular type of disturbance. Fig. 26 shows a comparison of the propagating stall speed at $\bar{\Phi} \cong 0.20$ (midway in the stall regime) with that for a full complement of blades. The stall speed in terms of the measured velocity fluctuation frequency is shown as a function of the rotor speed. The linear relationship between the propagating stall speed and the compressor rotor speed is evident here, and it is seen that decreasing the solidity by one-half decreased the propagation speed from 28 percent to 20 percent of the rotor speed.

Fig. 27 shows how the stall region width at mid-radius increased from 3 rotor blade channel widths at the start of stall to about 8 blade channels at the lower limit of propagating stall. Below this flow rate, the entire annulus evidently was in stall and it was impossible to detect any regularity in the velocity fluctuations. Fig. 28 illustrates the radial variation of the stall region width at a flow coefficient $\bar{\Phi} \cong 0.253$. The width is a maximum at the hub and is equivalent to the width of about 7 rotor blade channels, and a minimum at the outer radius where it is equivalent to about 3 rotor blade channel widths. Under these conditions, the width at mid-blade height is approximately equal to 4 blade channels.

The effect of removing the third stator row is shown in Fig. 25, where the propagating stall speed shows an increase throughout the propagating stall region except at the upper flow limit. At $\bar{\Phi} \cong 0.20$, this increase is from slightly under 20 percent to slightly above 22 percent of the rotor speed. This increase was similar to that observed with the full solidity. Removal of the third stator row also appeared to have the effect of maintaining a more constant stall speed throughout the propagating stall region. With full solidity for stator blades, one-half solidity for rotor blades and the third stator row in place, the propagating stall speed was 23 percent of the rotor speed (at $\bar{\Phi} \cong 0.20$).

V. COMPRESSOR STALL WITH ONE STAGE OF BLADING

5:1 One-Stage Free Vortex Blading

The regions of stall for the compressor with one stage of free vortex blading alone are shown in Fig. 29, which is a plot of the exit-duct wall pressure as a function of the flow coefficient. Stall initially occurred with closing throttle at the peak pressure point in the form of a single propagating stall region at the outside of the annulus rather than at the hub. This pattern commenced at $\bar{\Phi} \cong 0.31$ with a propagating stall speed of about 48 percent of the rotor speed as shown in Fig. 30. The single pattern had a maximum retarded flow region width of about 2 rotor blade channels and extended from the outer radius to about mid-blade height. Further throttling to $\bar{\Phi} = 0.303$ resulted in the formation of two stalled regions propagating at about the same speed as the single region, and placed 180 degrees apart in their most stable position. At $\bar{\Phi} = 0.298$, a single-region stall pattern again appeared with a lower propagation speed equal to about 36 percent of the rotor speed. From Fig. 30, it will be noted that the propagation speed for both types of partial stall decreases somewhat with closing throttle. The results of phase measurements made to determine the number of stalled regions for the foregoing cases are plotted in Fig. 31. It should be

noted that although the phase difference measured for a single stall cycle may be in considerable error due to instability of the flow, the average value of a number of a points for any position of the hot-wire probes gave very reasonable results. Each point in Fig. 31 represents the average value of five or more phase angle measurements.

Examples of the oscillograph records for the partial stall phenomena are given in Fig. 32. Fig. 33 is a plot of the velocity fluctuation amplitude ratio as a function of radius for the three afore-mentioned partial stall cases. For all the partial stall patterns, the velocity fluctuation amplitude ratio $\Delta V/\overline{V}$ was greatest at the tip ($\Delta V/\overline{V} \cong 0.6$), although for the lower flow one-region pattern a second maximum point of $\Delta V/\overline{V} \cong 0.6$ appeared at $R/R_o = 0.9$ or 1.8 inches from the tip. The first two partial stall patterns extended only to about mid radius as evidenced from the velocity fluctuations, however, the one-region pattern occurring at $\bar{\Phi} = 0.298$ showed a gradual decrease in velocity fluctuations towards the hub and did not diminish until a point very close to the hub. At the lower limit of this regime ($\bar{\Phi} \cong 0.26$), two-region stall patterns appeared, but they were rather unstable.

On further throttling to the flow coefficient range $0.26 > \bar{\Phi} > 0.11$, irregular velocity fluctuations were observed primarily in the outer part of the annulus.

Although this constituted stalling of the partial type, it was difficult to tell whether any propagation similar to the previous cases was involved. An example of the radial distribution of the velocity fluctuations for this regime is shown in Fig. 34 for the flow coefficient $\bar{\Phi} \cong 0.12$. The velocity fluctuations in this regime covered a greater portion of the compressor annulus than the previous cases, although it still decreased to a negligible value at the hub. The top chart in Fig. 35 is an example of the irregular velocity fluctuations found in this regime.

Full stall did not occur until $\bar{\Phi} \cong 0.11$ where a single region of retarded but fluctuating flow disturbance extending over the entire blade height appeared with the very low propagation speed of about 10 percent of the rotor speed. Examples of the velocity fluctuations found in this full stall regime are shown in the oscillograph records of Fig. 35. The retarded flow region does not appear to be caused by a single well-defined stall disturbance, but rather by a series of irregular stalled regions grouped together. The velocity fluctuations were very irregular in this retarded flow region, although investigations with an apparatus of higher frequency response might ascertain whether or not these fluctuations were a result of disturbances from all of the blades. The width of the fluctuating

retarded flow region increased towards the outer radius, and in Fig. 36 this radial variation is plotted for a flow coefficient $\bar{\Phi} = 0.112$. At this flow rate, the region of retarded flow had a width of about 6 rotor blade channels at the hub and increased to cover the entire annulus at the tip. The peak velocity fluctuation amplitude ratio did not vary radially to a great extent (see Fig. 34), having a maximum value of about 0.6 at mid-blade height.

Closing the throttle further (from $\bar{\Phi} = 0.112$) increased the width of the region of retarded flow at the hub from 6 rotor blade channel widths to about 22 channel widths at $\bar{\Phi} = 0.075$ (see Fig. 37). Below this flow rate, irregular flow seemed to occur over the entire annulus. In terms of audible noise, a definite periodic beat could be heard when the compressor was in full stall, but only a continuous rumbling sound was noticeable below this regime.

When the throttle was opened from shut-off, the sequence of stall phenomena appeared in reverse order but at slightly higher flow rates (see Fig. 29). The exit-duct wall pressure values were slightly lower going out of full stall than when the throttle was being closed, however, this was the only point at which the exit-duct wall pressure showed any hysteresis effect.

5:2 One-Stage Solid Body Blading

With one stage of solid body blading, the stall occurred first in the outer part of the annulus as the compressor was throttled. Fig. 38, which plots exit-duct wall pressure as a function of flow coefficient, shows that propagating stall initially occurs at about the point of maximum exit-duct pressure at a flow coefficient $\bar{\Phi} \cong 0.31$. The top chart in Fig. 39 is an example of the type of velocity fluctuation existing at the initial stall point. The stall patterns at the tip ($R/R_o = 0.98$) were rather unstable so that consistent determinations of frequency were impossible. However, the initial stall appearing at $\bar{\Phi} \cong 0.31$ tended to be one with a propagating speed of about 45 percent of the rotor speed. Upon closing the throttle to the flow coefficient $\bar{\Phi} \cong 0.30$, no very stable pattern appeared although there was some evidence of a pattern with two regions of retarded flow. Further throttling beyond the flow coefficient $\bar{\Phi} \cong 0.27$, gave only irregular fluctuations of the flow velocities concentrated, for the most part, in the outer portion of the annulus. This behavior was quite similar to that observed with one stage of free vortex blading. The exit-duct wall static pressure decreased gradually from its maximum value with closing throttle until $\bar{\Phi} \cong 0.13$ where full stall first appeared. There were no distinct variations in the exit-duct wall

pressure in the partial stall region as was observed with one stage of free-vortex blading, just as there were no distinct types of partial stall patterns.

In Fig. 40, the radial variation of the velocity fluctuation amplitude ratio, $\Delta V/\overline{V}$, is shown for the initial unstable one-region partial stall at $\bar{\Phi} \cong 0.31$ and also for the unstable two-region partial stall occurring at $\bar{\Phi} \cong 0.30$. The velocity fluctuations are a maximum at the tip and decrease rapidly from $R/R_o = 0.9$ towards the hub. Similar to the partial stall cases for the other blade configurations, the maximum value of $\Delta V/\overline{V}$ was about 0.6. The velocity fluctuation ratio for the irregular partial stall regime ($0.27 > \bar{\Phi} > 0.13$) had about the same variation as that for one-stage free vortex blading, however, the maximum value of $\Delta V/\overline{V}$ remained constant over a larger portion of the annulus. This is illustrated for the flow coefficient $\bar{\Phi} \cong 0.16$ in Fig. 41.

Full stall occurred at $\bar{\Phi} \cong 0.13$ upon closing the throttle with one region of retarded fluctuating flow propagating in the direction of compressor rotation with a speed of about 12 percent of the rotor speed. The velocity fluctuations for full stall were similar to those observed with one stage of free vortex blading, as shown on the bottom row of chart records in Fig. 39. The velocity fluctuation amplitude ratio remained fairly constant

over the compressor radius and had a maximum value, $\Delta V/\overline{V} \cong 0.65$ (see Fig. 41). The propagating stall speed decreased with closing throttle to about 9 percent of rotor speed at the lower flow limit of full stall, as shown in Fig. 42.

As for the single-stage free vortex blading, the width of the retarded flow region near the hub increased on closing the throttle from 9 rotor blade channel widths to extend over the entire annulus at $\bar{\Phi} \cong 0.050$ (see Fig. 43). In Fig. 44, the radial variations of the retarded flow region width are shown for two cases, one for the highest flow rate in full stall and the other near the lower flow rate limit. In both cases, the retarded flow region was a minimum at the hub and increased to cover the entire circumference at about $R/R_o = 0.9$, then decreased again to cover approximately 20 rotor blade channel widths at the tip.

Closing the throttle below $\bar{\Phi} \cong 0.050$ brought irregular flow throughout the annulus which made determinations of definite flow patterns impossible. The exit-duct wall pressure increased slightly at this point as shown in Fig. 38. Similar to the case for the free vortex blading, on opening the throttle, the reverse sequence of stall phenomena occurred at slightly higher flow coefficients than when the throttle was being closed. The exit-duct wall pressure had a lower value going out

of full stall than when the flow was being throttled, and this was the only hysteresis effect observed in the exit-duct pressure characteristic.

VI. SUMMARY OF THE EXPERIMENTAL RESULTS

Propagating stall occurred in the form of more or less well-defined regions of retarded flow which rotated without changing shape in the direction of blade rotation with a speed proportional to, but of smaller magnitude than, the rotor speed. Two principal types of stall were observed which are defined as "Partial Stall" and "Full Stall".

Partial Stall characteristics are:

1. Partial stall occurs at higher flow coefficients than full stall.
2. The stalled region or regions extend over only a part of the blade height.
3. One or more stalled regions may exist.
4. The stalled region may be concentrated either at the root or the tip, depending on the blade and compressor configuration.
5. The propagating stall speed is higher than that for the full stall type.
6. Transition into partial stall upon closing the throttle occurs at or slightly beyond the maximum exit-duct pressure and is accompanied by a small or gradual decrease in pressure.
7. The size of the stalled region or regions increases with decrease in flow coefficient until a transition point is reached where one of

the following happens:

a. The region or regions regroup into the next larger number of regions propagating at about the same speed.

b. The multiple-region pattern regroups into one partial stall region propagating with a lower speed (this was found for one-stage free-vortex blading).

c. The partial stall regions regroup into a single region of the full stall type.

8. The maximum velocity fluctuation amplitude ratio, $\Delta V/\overline{V}$, was about the same for all cases ($\Delta V/\overline{V}$ = 0.6 to 0.65).

Full Stall characteristics are:

1. The stalled region extends over the full blade height.
2. Only one stalled region exists.
3. The propagating stall speed is lower than that for partial stall.
4. Transition into full stall is accompanied by a drop in exit-duct pressure upon closing the throttle, and a hysteresis loop is found when exit-duct pressure variations for opening and closing throttle are compared.
5. The propagating stall speed does not change appreciably with flow coefficient.

6. The propagating stall speed is reduced with a decrease in solidity (three-stage free vortex blading).
7. The size of the retarded flow region increases with decrease in flow coefficient.
8. At any given flow coefficient in the full stall regime, the retarded flow region is widest at the radial position where partial stall is widest.
9. The maximum value of the velocity fluctuation amplitude ratio, $\Delta V/\overline{V}$, is about 0.7

All stall phenomena observed were not of the well-defined propagating stall type. Results from one stage tests indicated a partial stall which was not well-defined, and at very low flow coefficients a poorly-defined full stall. It is not certain whether the irregular velocity fluctuations observed in these instances result from the propagating stall, a high frequency surge, or a combination.

VII. DISCUSSION OF THE EXPERIMENTS

The general characteristics of propagating stall brought out by the experimental results seem to be in agreement with those reported by Huppert and Benser (Ref. 4), where the partial stall and full stall are called respectively, "progressive stage stall" and "root-to-tip stage stall". Apparently they observed only multiple stall regions for the partial stall case, whereas for the compressor configurations tested here, partial stall initially started with one retarded flow region which then increased in number with decrease in flow coefficient. In the case of full stall, both results indicated the presence of only one stalled region. The most significant difference between partial and full stall cited by these investigators was the gradual decrease in pressure coefficient associated with partial stall as compared with the discontinuity of pressure coefficient (and accompanying hysteresis characteristic) in the case of full stall. This also was found in the experiments conducted, as in the case of three-stage free vortex blading where a distinct hysteresis loop was formed in the transitions between partial and full stall. Smaller loops were found in the one-stage configurations. It would be expected that a different characteristic line of static pressure rise versus flow coefficient would be found for each distinct type of stall pattern.

The transition from one stall pattern to another occurred at different flow rates, depending on whether the flow was being increased or decreased, hence hysteresis loops should be found at these transition points. In the case of the transitions of the multiple patterns in the partial stall, no hysteresis loops were detected although they undoubtedly exist even if small.

Huppert and Benser also point out the importance of system damping on the compressor surge or stable characteristics. If the receiver volume is large as was in the case of their test unit, the damping coefficient would be small and the compressor quite likely to surge. In the experiments described here, the external volume was relatively small and the compressor stalled rather than surged. The existence of a hysteresis loop is one of the conditions for surging, hence it is probable that surging involves an oscillation between two different stall patterns. The surging frequency is usually, if not always, the natural frequency of the resonator connected with the compressor. If surging occurred it would be difficult to trace out a hysteresis characteristic because of the overall flow fluctuating with time, consequently stall characteristics undoubtedly would be hard to obtain. At present, it is not clear what the conditions are for occurrence of self-induced oscillations and their amplitudes resulting from the presence of the hysteresis loops.

The complicated nature of the various propagating stall patterns makes it impossible to give any detailed explanation at the present time. Theoretical studies of propagating disturbances in two-dimensional cascades have been made recently by Sears (Ref. 9) and Marble (Ref. 10). Sears assumed an infinite number of blades, and although Marble treated the case of a finite number, this refinement amounts to only a small correction. Both investigations were based on perfect fluid flow but with different assumptions concerning the behavior of the unsteady lift with angle of attack. Sears introduced a phase lag between a sinusoidal circulation (representing the fluctuating lift) and the mean angle of incidence which gave asymmetric sinusoidal solutions leading to a disturbance propagation. The blade characteristic (lift coefficient as a function of angle of attack) was assumed linear in this case. Marble introduced a non-linear dependence of lift on angle of attack and on rate of change of angle of attack so that a hysteresis loop was formed, and found the propagating speed in terms of an arbitrary characteristic time in the lift relation.

In both of the above theories, the characteristic time was undetermined. It was believed that this was connected with the time required for establishment of a separated boundary layer when an airfoil of the cascade was subjected to a sudden change of angle of attack.

Mendelson (Ref. 11) determined the phase lag of the circulation with angle of attack from experiments on various single airfoils, and concluded that to the first approximation, at least, it depends on the lift coefficient and not on the frequency of oscillation. The phase lags reported were about one radian near the stall, and Sears showed that the lag required to have propagating stall was about this magnitude. However, there is no precise correspondence and some of the results from the compressor experiments seem rather inconsistent with a characteristic time of this type. For instance, if the above were correct, removal of every second blade in the compressor should result in doubling the stall propagating speed, but no such result was observed. The presence of more than one blade row may influence the results although the speed variation trend is opposite to that predicted by the theory.

Rannie has suggested that a more realistic picture of the stall propagation through cascades of moderate or high solidity can be gained by concentrating attention on the leaving flow angle and the total pressure loss through the cascade. To a first approximation, the leaving angle can be assumed independent of the incidence angle even in stalled operation. This would be simpler to use than the lift coefficient corrected for cascade interference. The total pressure loss is small and approximately constant

over a range of incidence angle of 8° to 10°, but rises sharply outside this range. The propagating stall phenomenon is typical of non-linear oscillations, and inasmuch as the most marked non-linear characteristic of the flow is found in the total pressure loss variation, Rannie believes that this characteristic is important in determining the amplitudes of the stall fluctuations.

Although the characteristic time controlling the propagating speed are not determined by a knowledge of the leaving angle and the total pressure loss as functions of the incidence angle, this representation of the cascade flow has a broader scope and seems to have advantages over the earlier approaches of Sears and Marble. At Rannie's suggestion, Sears made an analysis (Ref. 12) based on the relationship between the total pressure rise and the leaving angle of the flow which was assumed constant. This was introduced in place of the airfoil lift characteristics used in his earlier analysis. Further, he generalized the relations by introducing the same phase lag used in the earlier airfoil case. These assumptions also led to families of asymmetric flow patterns both with and without the time lag. However, he approximated the total pressure rise versus incidence angle relation by a linear function, so the total pressure loss was not introduced and neither the amplitudes of the fluctuations nor the propagating speed were determined.

The full stall propagating speed was relatively constant over a wide flow coefficient range which would require a characteristic time rather insensitive to large changes of mean angle of incidence and even to reversed flow. This seems inconsistent with the time required for establishment of a boundary layer. The results seem to indicate a characteristic time that is relatively independent of the number of blades and of the detailed nature of the flow through the blades. Therefore, a characteristic time connected with the inertia (or apparent mass) of the flow approaching the cascade has been suggested as more reasonable than that based on the boundary layer establishment. At present, Marble is making an analysis based on these assumptions. The shifting of the streamlines far in front of the cascade by the alternate stalling and unstalling of the cascade should not be strongly dependent on the cascade solidity or the detailed nature of the flow itself. Certainly, more experimental evidence is required to show definitely that the inertia effect does determine the characteristic time. Also, the presence of more than one blade row may influence the experimental results, hence a study of a single rotor blade alone is necessary.

Since both rotor and stator rows were involved in the propagating disturbances, it is not certain which was primarily responsible. There was some tendency for the width

of the retarded flow region to be integral multiples of the rotor blade channel widths at the hub and blade tip in full stall, and therefore there is reason for believing that the disturbances were propagating on the rotor. The stator blades had a very definite influence in determining the characteristics of the propagating stall. First, it seemed to influence whether or not a given stall pattern occurred, as demonstrated by the results of removing the third stator row. This prevented the multiple patterns at the hub from occurring, even five blade rows ahead. Also, removal of the third stator row seemed to have the effect of maintaining a more constant propagation speed in the full stall regime and of increasing the stall speed over that found with the full complement of blades.

The full stall regime was the most stable as far as range of flow was concerned (at least with more than one stage installed), and the two-dimensional theoretical approaches mentioned previously are applicable only for the full stall case. However, an understanding of the partial stall phenomena is perhaps more important. The partial stall occurs at the larger flow rates and would be more apt to occur in turbojet operation than the full stall because of its proximity to the stall point. Blade failures would be more likely to occur in the partial stall region or at the flow rates corresponding to the beginning of stall. Previously, it has been believed that blade failure was caused primarily by a stalled flutter

with only one mode of vibration excited by the self-induced aerodynamic forces. However, the existence of partial stall disturbances can create large aerodynamic excitation without a self-induced flutter of the blades, and it is possible that partial stall may be responsible for blade failure rather than the stalled flutter. The flexibility of the compressor blades may have some effect on the partial stall. Since the observed partial stall patterns were of a metastable type, a blade natural frequency in the range of the partial stall frequencies might influence the relative stability of the partial stall regimes. From the standpoint of reducing aerodynamic excitation of the rotor blades, it would be preferable to have the partial stall occur at the hub rather than the blade tip. The free vortex rotor blades have constant chord from root to tip although this is not the general practise. While partial stall occurred at the hub in the three-stage tests, it might well occur at the tip with the more conventional tapering blades (less solidity at tip). The conditions for the occurrence of tip stall are not clearly understood, although it undoubtedly is influenced by the hub ratio of the compressor.

The effective wave lengths of the partial stall and even more of the full stall patterns are so large that the influence of the propagating stall cannot be confined to a single blade row, because the distance between center

lines of the blade rows is a small fraction of the pattern wave length. Hence, stall on a single blade row can influence both rows far ahead and far behind.

VIII. REFERENCES

1. "Aerodynamic Problems in Axial Compressors for Aircraft Jet Engines" by R. S. Hall, Institute of the Aeronautical Sciences, Preprint No. 216, May 1949.

2. "Surging in Centrifugal and Axial-Flow Compressors" by R. O. Bullock and H. B. Finger, Society for Automotive Engineers, Preprint No. 605, Presented at SAE National Aeronautical Meeting, New York City, April 1951.

3. "Surging of Axial Compressors" by H. Pearson and T. Bowmer, The Aeronautical Quarterly, Vol. 1, November 1949, pp. 195-210, Royal Aeronautical Society, London.

4. "Some Stall and Surge Phenomena in Axial-Flow Compressors", by M. C. Huppert and W. A. Benser, NACA, preprint of paper presented at the 21st Annual Meeting of the Institute of Aeronautical Sciences, New York City, January, 1953.

5. "Theoretical and Experimental Investigations of Axial Flow Compressors", by J. T. Bowen, R. H. Sabersky, and W. D. Rannie, Report on Research Conducted under Contract with the Office of Naval Research, California Institute of Technology, January, 1949.

6. "Theoretical and Experimental Investigations of

Axial Flow Compressors, Part 3, Progress Report on Loss Measurements in Vortex Blading", by C. C. Alsworth and T. Iura, Report on Research Conducted under Contract with the Office of Naval Research, California Institute of Technology, July, 1951.

7. "Investigations of Axial-Flow Compressors", by J. T. Bowen, R. H. Sabersky, and W. D. Rannie, Transactions of the ASME, Vol. 73, No. 1, January, 1951, pp. 1-15.

8. "Review of Hot-Wire Anemometry", by J. B. Willis, Australian Council for Aeronautics Report ACA-19, October, 1945.

9. "On Asymmetric Flow in an Axial-Flow Compressor Stage", by W. R. Sears, ASME Preprint, Paper No. 52-F-15, presented at ASME Fall Meeting, September, 1952.

10. "Propagation of Stall in Compressor Blade Rows", by F. E. Marble, California Institute of Technology, paper presented at Institute of Aeronautical Sciences' 21st Annual Meeting, New York City, January, 1953.

11. "Effect of Aerodynamic Hysteresis on Critical Flutter Speed at Stall", by A. Mendelson, NACA Research Memorandum No. E8304, June 1948.

12. "A Theory of 'Rotating Stall' in Axial-Flow Compressors", by W. R. Sears, Report under Contract AF 33 (038) - 21406, Graduate School of Aeronautical Engineering, Cornell University, 1953.

IX. NOMENCLATURE

The following nomenclature was used in this report:

Symbol		Definition
A	=	compressor annulus area
C_a	=	axial velocity component
$\overline{C}_a$	=	axial velocity component averaged over the annulus
C_u	=	tangential velocity component
L	=	cycle length of velocity fluctuation
N_P	=	number of propagating stall regions
R	=	hot-wire resistance
R_a	=	wire resistance at air temperature
R_o	=	wire resistance at 0^o C
V	=	instantaneous velocity normal to radius of compressor
$\overline{V}$	=	mean velocity normal to radius of compressor
a,b	=	constants
c	=	airfoil chord length
i	=	heating current for hot-wire
p_s	=	static pressure
p_a	=	atmospheric pressure
r, R	=	radius of a particular stream tube
r_i, R_i	=	hub radius
r_o, R_o	=	tip radius

s = cascade pitch

u_o = velocity of rotor blade tip

Δ = change of a quantity

α = temperature coefficient of resistance of the wire material

ρ = fluid density

$\bar{\phi}$ = average flow coefficient = $\bar{C}_a/u_o$

ω = rotor angular velocity

ω_s = stalled region angular velocity

$\bar{\psi}$ = average power coefficient = $\dfrac{\text{Shaft Power}}{1/2\ \rho A \bar{C}_a u_o^2}$

FREE VORTEX $\left[C_{u1} = .145 \frac{r_0}{r} u_0 ;\ C_{u2} = .345 \frac{r_0}{r} u_0\right]$

	ROTOR					STATOR				
SECTION LOCATION - r - INCHES	10.8	12.6	14.4	16.2	18.0	10.8	12.6	14.4	16.2	18.0
DESIGN ENT. ANGLE - ROTOR - β_1 - DEG.	51° 21′	42° 24′	36° 2′	31° 21′	27° 45′					
DESIGN ENT. ANGLE - STATOR - γ_2 - DEG.						38° 3′	42° 24′	46° 13′	49° 34′	52° 31′
DESIGN EXIT ANGLE - ROTOR - β_2 - DEG.	86° 49′	65° 17′	50° 40′	41° 3′	34° 29′					
DESIGN EXIT ANGLE - STATOR - γ_1 - DEG.						61° 46′	65° 17′	68° 4′	70° 18′	72° 8′
SECTION CAMBER - θ - DEGREES	46° 40′	31° 0′	20° 19′	13° 47′	9° 48′	31° 53′	31° 6′	29° 59′	28° 41′	27° 20′
CASCADE STAGGER ANGLE - β' - DEG.	74° 48′	57° 54′	46° 12′	38° 15′	32° 36′					
CASCADE STAGGER ANGLE - γ - DEG.						54° 0′	57° 57′	61° 12′	63° 55′	66° 11′
SOLIDITY - C/S	1.150	.985	.862	.766	.690	1.035	.970	.920	.880	.849
MAXIMUM THICKNESS - % C	12	11	10	9	8	10	10	10	10	10

SOLID BODY $\left[C_{u1} = .325 \frac{r}{r_0} u_0 ;\ C_{u2} = \left(.325 \frac{r}{r_0} + .200 \frac{r_0}{r}\right) u_0\right]$

	ROTOR					STATOR				
SECTION LOCATION - r - INCHES	10.8	12.6	14.4	16.2	18.0	10.8	12.6	14.4	16.2	18.0
DESIGN ENT. ANGLE - ROTOR - β_1 - DEG.	52° 10′	46° 18′	40° 30′	34° 42′	28° 43′					
DESIGN ENT. ANGLE - STATOR - γ_2 - DEG.						48° 22′	46° 15′	42° 40′	37° 2′	29° 18′
DESIGN EXIT ANGLE - ROTOR - β_2 - DEG.	83° 7′	70° 47′	58° 19′	45° 33′	31° 48′					
DESIGN EXIT ANGLE - STATOR - γ_1 - DEG.						69° 30′	65° 18′	60° 36′	55° 11′	48° 41′
SECTION CAMBER - θ - DEGREES	40° 52′	32° 45′	24° 6′	14° 49′	4° 15′	28° 23′	25° 53′	24° 37′	24° 42′	27° 0′
CASCADE STAGGER ANGLE - β' - DEG.	72° 36′	62° 41′	52° 33′	42° 7′	30° 51′					
CASCADE STAGGER ANGLE - γ - DEG.						62° 34′	59° 12′	54° 59′	49° 42′	42° 48′
SOLIDITY - C/S	1.150	1.061	.995	.944	.903	1.039	.970	.920	.880	.850
MAXIMUM THICKNESS - % C	12	11	10	9	8	10	10	10	10	10

Table 1 Geometric Properties of the Blade Sets

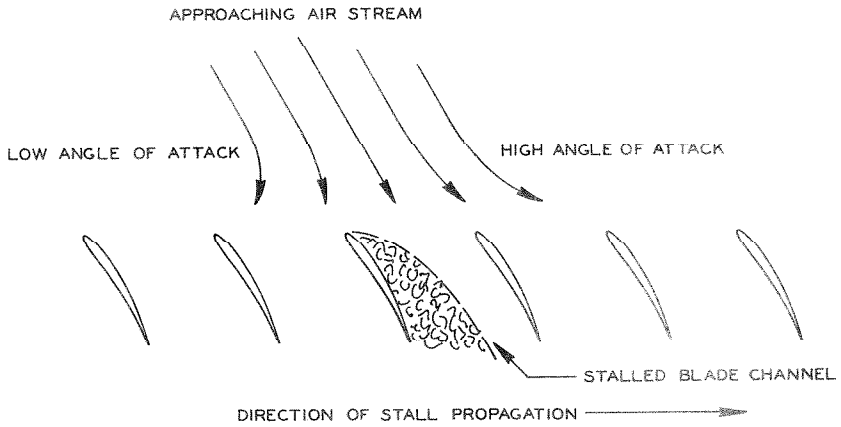

Fig. 1: Stall Propagation in a Cascade

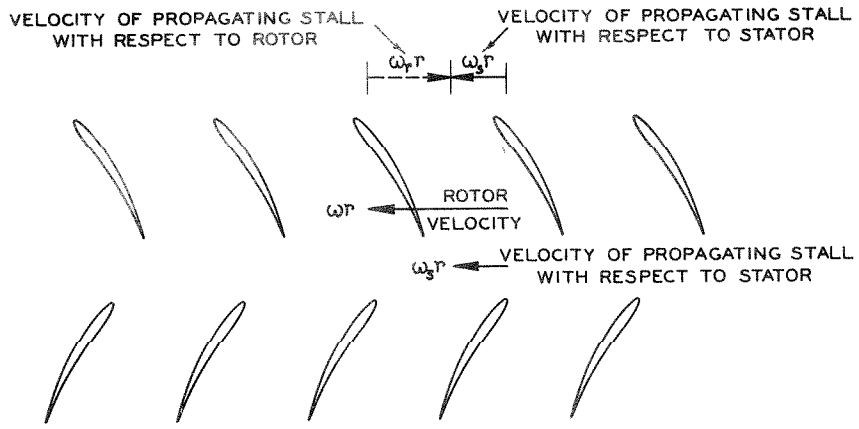

Fig. 2: Stall Propagation in Compressor Blade Rows

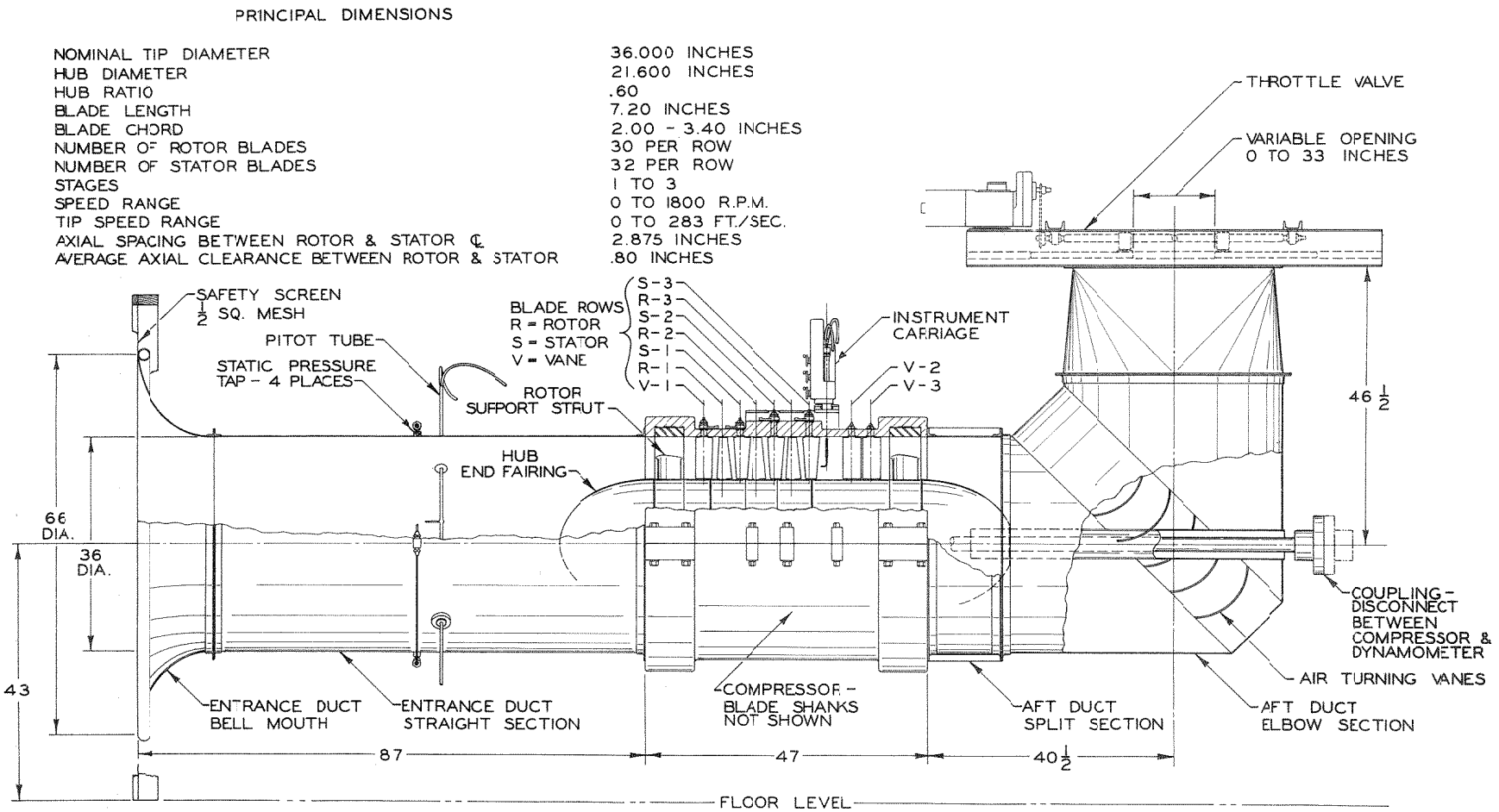

Fig. 3: Assembly Drawing of the Test Installation

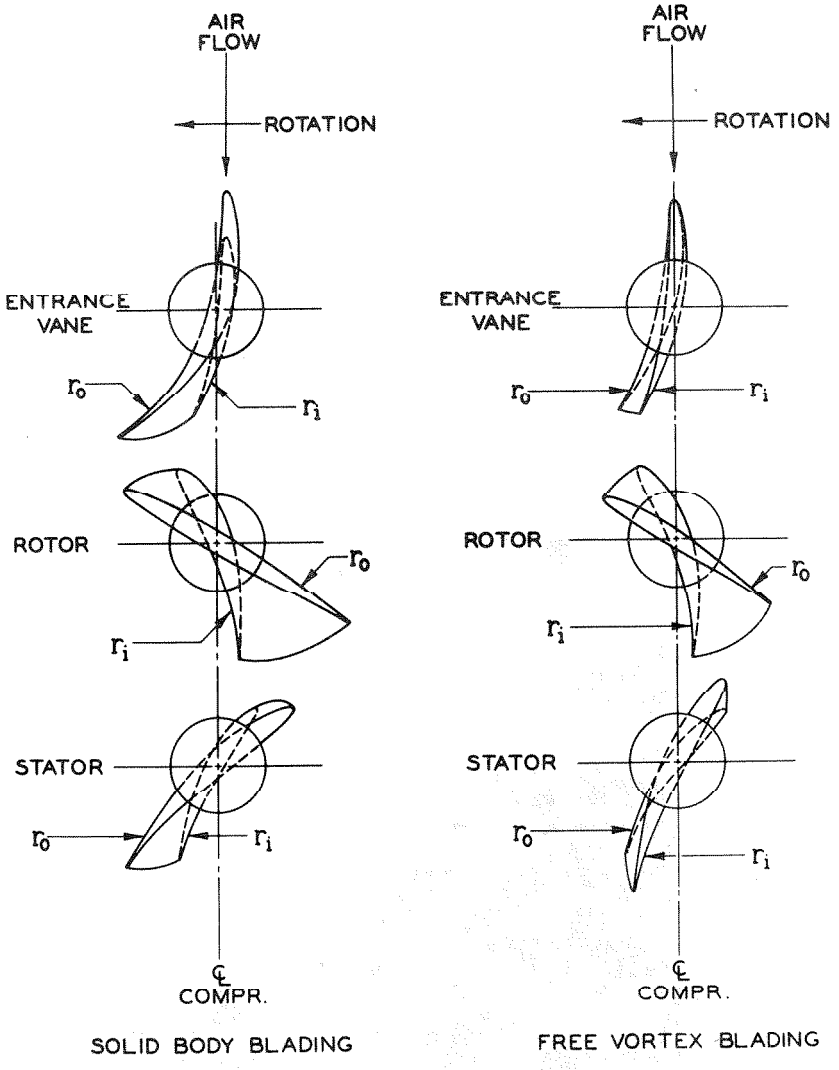

Fig. 4: Root and Tip Sections of the Two Types of Compressor Blading

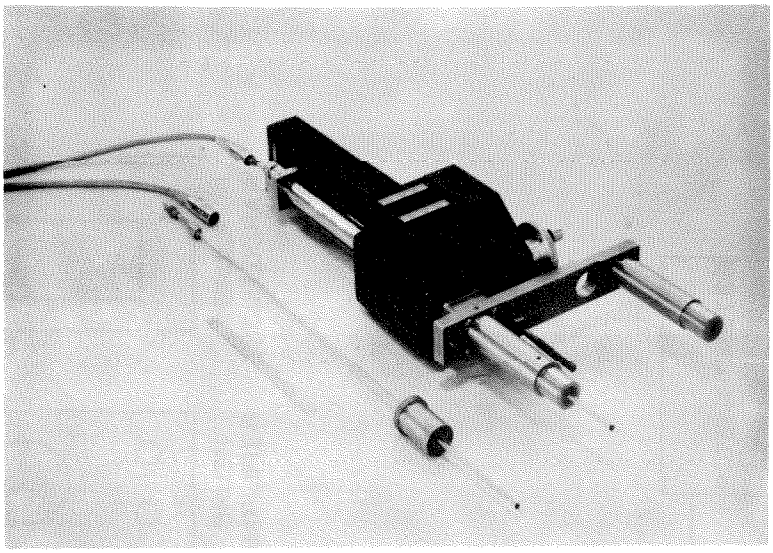

Fig. 5: Hot Wire Anemometer Probes and Radial Survey Carriage

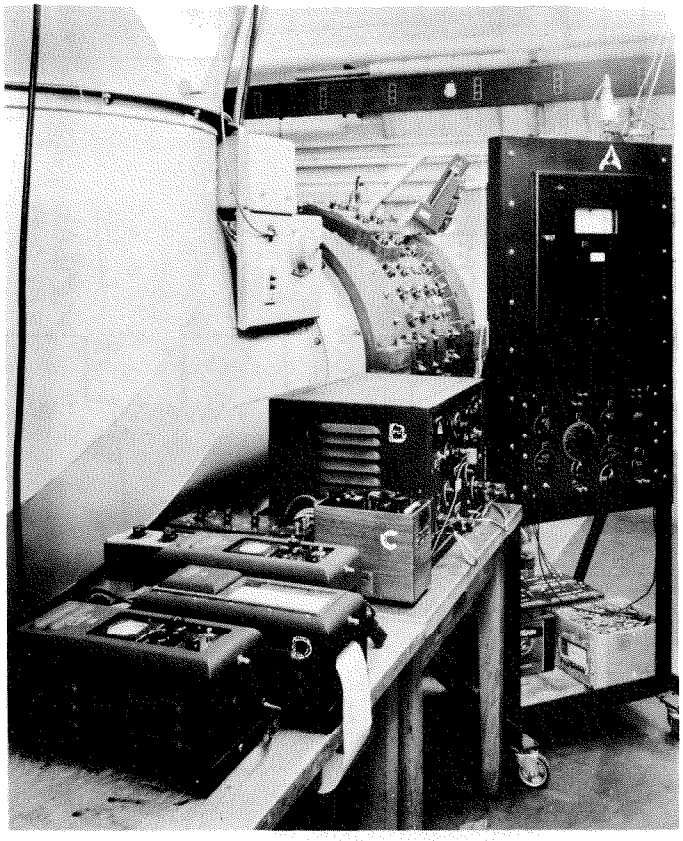

Fig. 6: General View of Instruments: (A) Pressure Detecting Unit, (B) Hot-Wire Heating Circuit and Amplifier, (C) Potentiometer, (D) Oscillograph

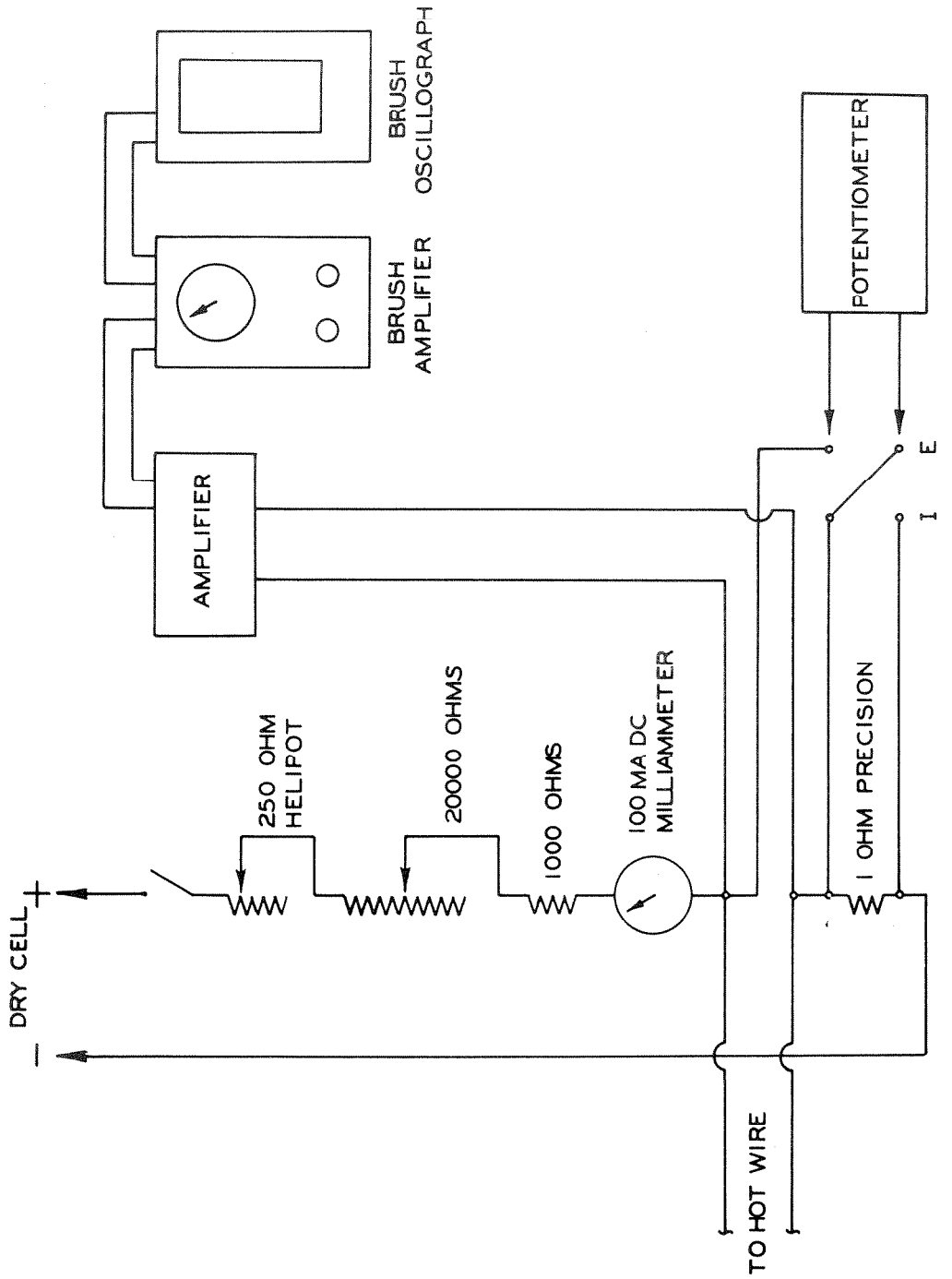

Fig. 7: Schematic Diagram of Hot Wire Apparatus

FIGURE 8
CALIBRATION CURVE OF 0.00024 INCH PLATINUM WIRE
FOR CONSTANT CURRENT OPERATION
PLOTTED FOR CONFORMITY WITH KING'S EQUATION

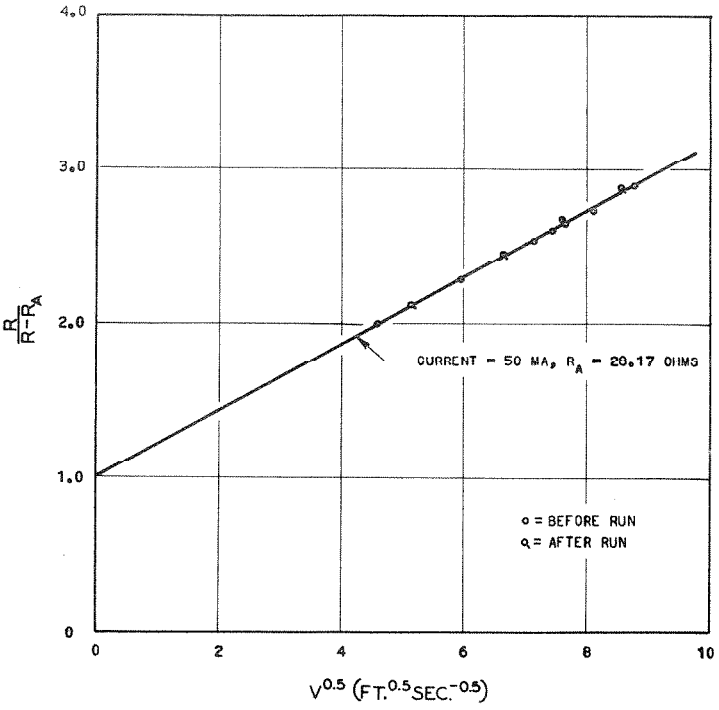

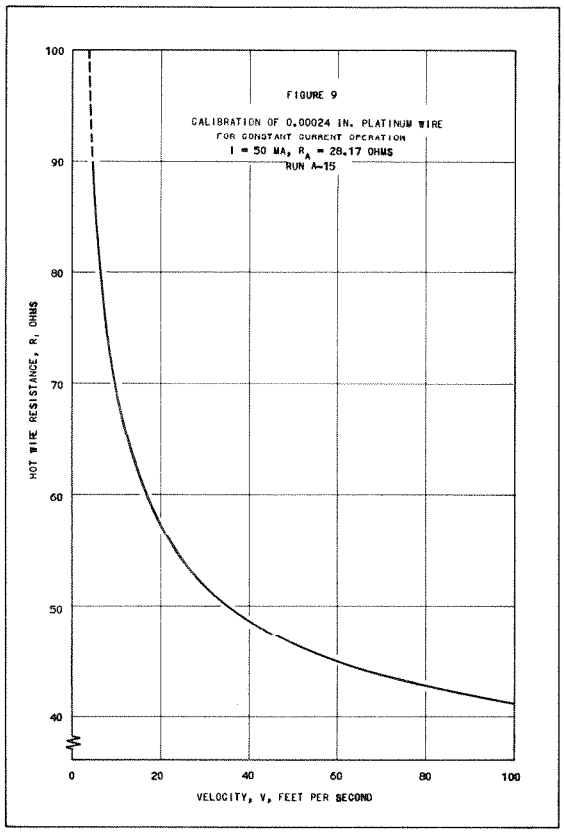

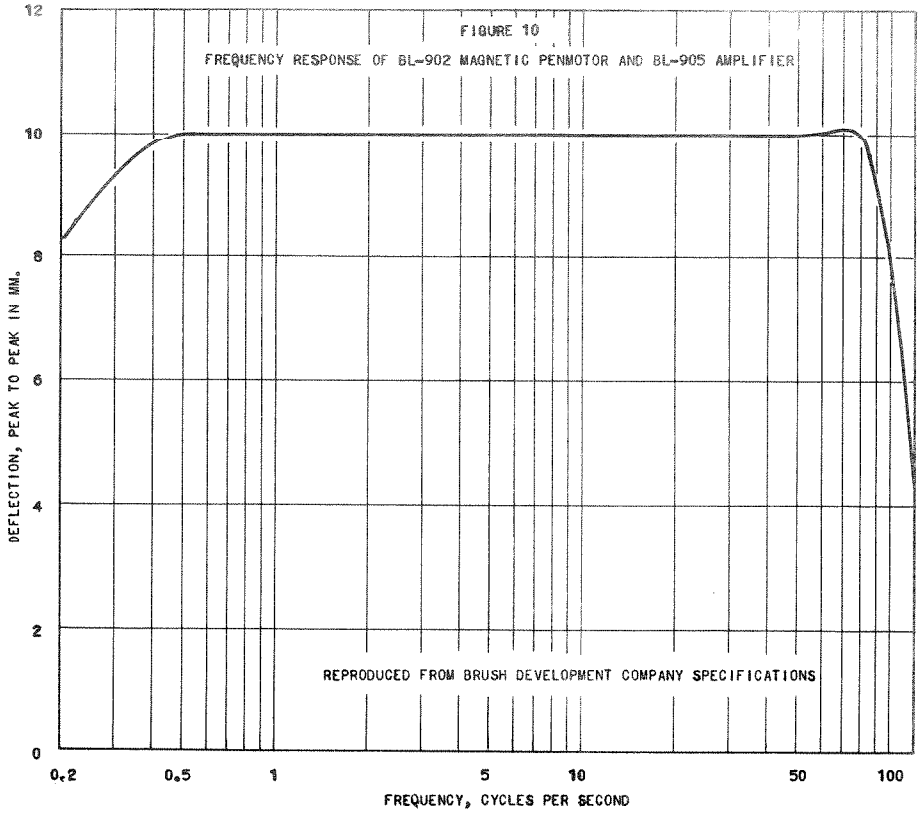
FIGURE 10
FREQUENCY RESPONSE OF BL-902 MAGNETIC PENMOTOR AND BL-905 AMPLIFIER
REPRODUCED FROM BRUSH DEVELOPMENT COMPANY SPECIFICATIONS
DEFLECTION, PEAK TO PEAK IN MM.
FREQUENCY, CYCLES PER SECOND
0
2
4
6
8
10
12
0.2
0.5
1
5
10
50
100

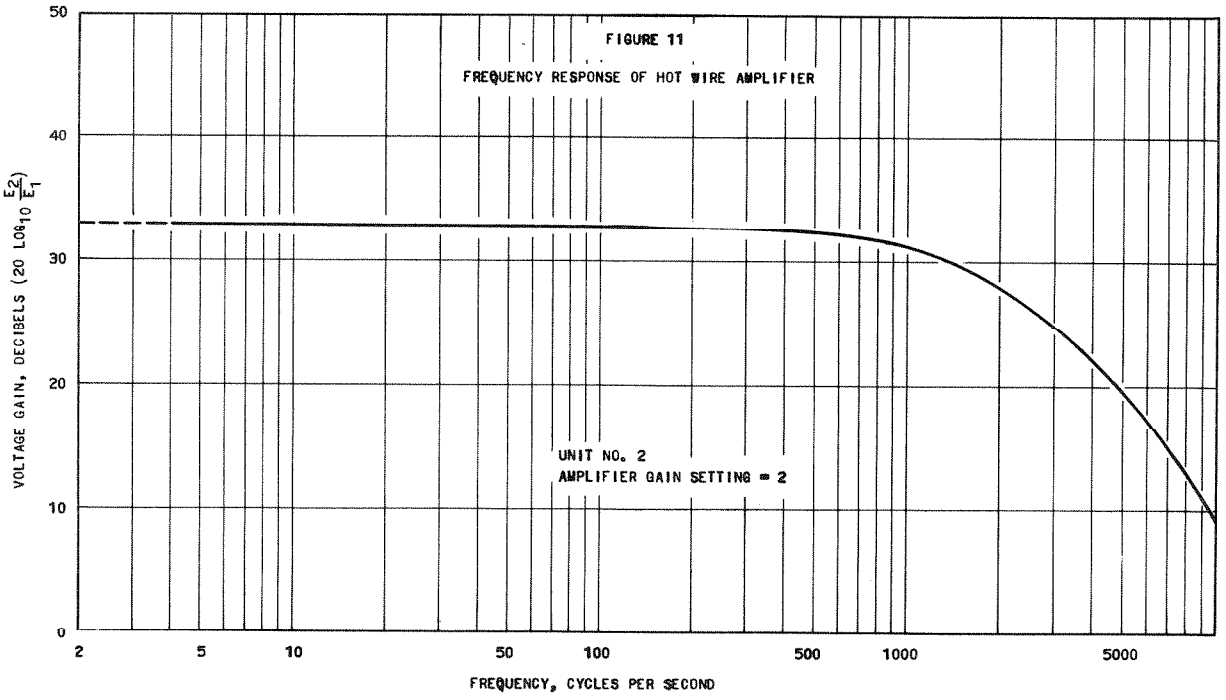
FIGURE 11
FREQUENCY RESPONSE OF HOT WIRE AMPLIFIER
UNIT NO. 2
AMPLIFIER GAIN SETTING = 2
VOLTAGE GAIN, DECIBELS (20 LOG10 E2/E1)
FREQUENCY, CYCLES PER SECOND
0
10
20
30
40
50
2
5
10
50
100
500
1000
5000

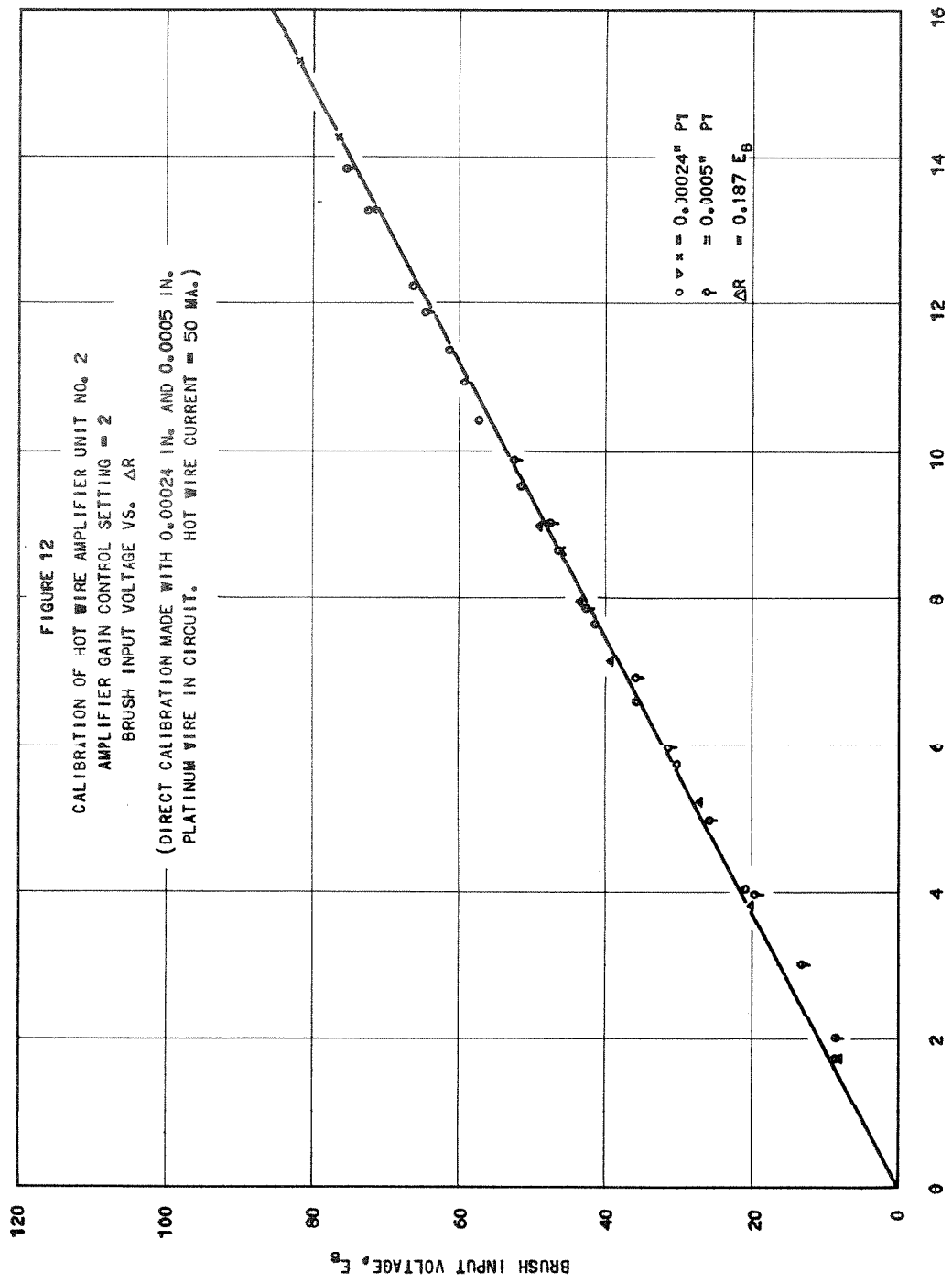
FIGURE 12
CALIBRATION OF HOT WIRE AMPLIFIER UNIT NO. 2
AMPLIFIER GAIN CONTROL SETTING = 2
BRUSH INPUT VOLTAGE VS. ΔR
(DIRECT CALIBRATION MADE WITH 0.00024 IN. AND 0.0005 IN.
PLATINUM WIRE IN CIRCUIT. HOT WIRE CURRENT = 50 MA.)
o ▽ x = 0.00024" Pt
ρ = 0.0005" Pt
ΔR = 0.187 E_B
BRUSH INPUT VOLTAGE, E_B
CHANGE IN RESISTANCE, ΔR, OHMS
0
20
40
60
80
100
120
0
2
4
6
8
10
12
14
16

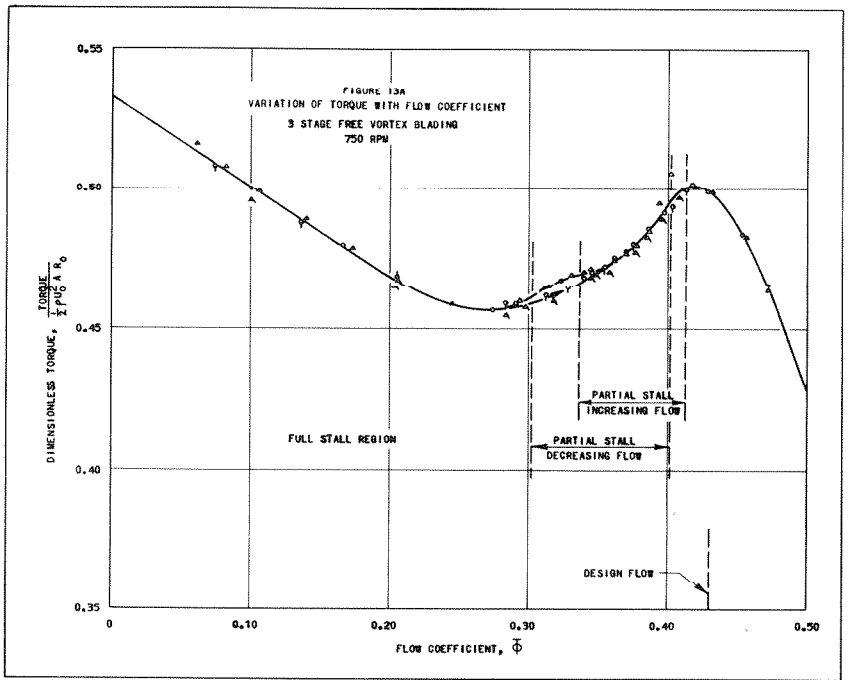
FIGURE 13A
VARIATION OF TORQUE WITH FLOW COEFFICIENT
3 STAGE FREE VORTEX BLADING
750 RPM
DIMENSIONLESS TORQUE, $\frac{\text{TORQUE}}{\frac{1}{2}\rho U_0^2 A R_0}$
0.55
0.50
0.45
0.40
0.35
FULL STALL REGION
PARTIAL STALL
INCREASING FLOW
PARTIAL STALL
DECREASING FLOW
DESIGN FLOW
0
0.10
0.20
0.30
0.40
0.50
FLOW COEFFICIENT, Φ

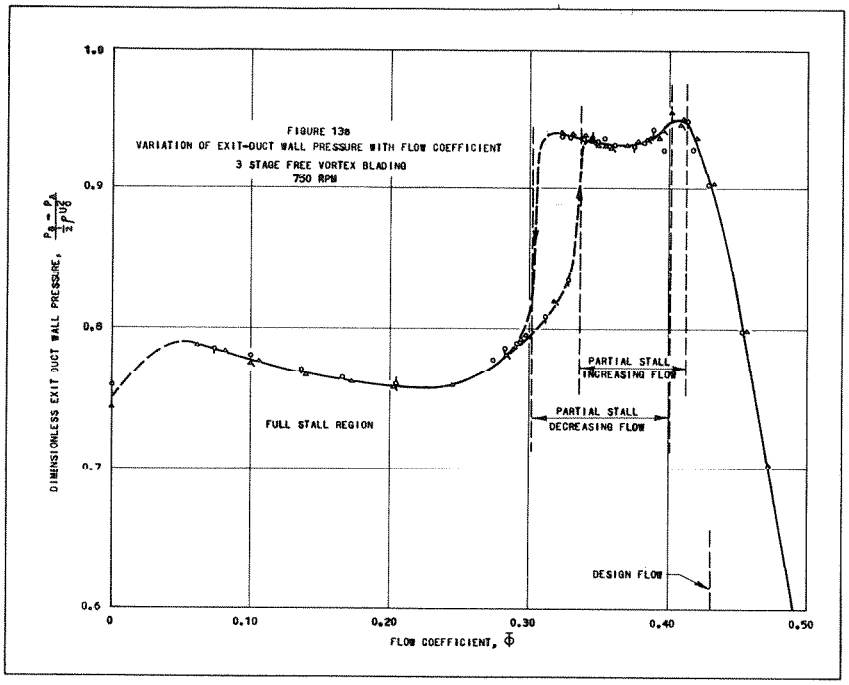
FIGURE 13B
VARIATION OF EXIT-DUCT WALL PRESSURE WITH FLOW COEFFICIENT
3 STAGE FREE VORTEX BLADING
750 RPM
DIMENSIONLESS EXIT DUCT WALL PRESSURE, $\frac{p_B - p_A}{\frac{1}{2}\rho U_0^2}$
1.0
0.9
0.8
0.7
0.6
FULL STALL REGION
PARTIAL STALL
INCREASING FLOW
PARTIAL STALL
DECREASING FLOW
DESIGN FLOW
0
0.10
0.20
0.30
0.40
0.50
FLOW COEFFICIENT, Φ

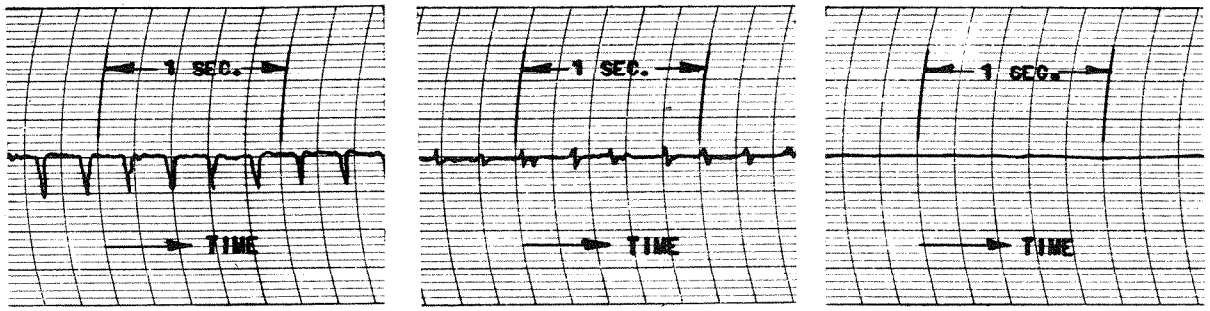

$R/R_0 = 0.65$ $R/R_0 = 0.75$ $R/R_0 = 0.80$

ONE-REGION PARTIAL STALL, $\bar{\Phi} = 0.397$, INITIAL STALL POINT AT CLOSING THROTTLE, PROPAGATING STALL SPEED = 38 PERCENT OF ROTOR SPEED

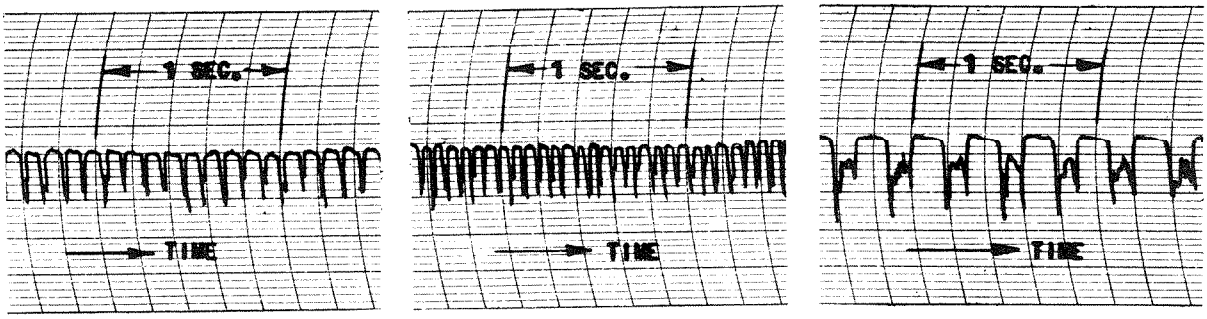

TWO-REGION PARTIAL STALL
$\bar{\Phi} = 0.38$, $R/R_0 = 0.65$
$\omega_s = 0.38\,\omega$

THREE-REGION PARTIAL STALL
$\bar{\Phi} = 0.36$, $R/R_0 = 0.65$
$\omega_s = 0.38\,\omega$

FULL STALL
$\bar{\Phi} = 0.29$, $R/R_0 = 0.65$
$\omega_s = 0.26\,\omega$

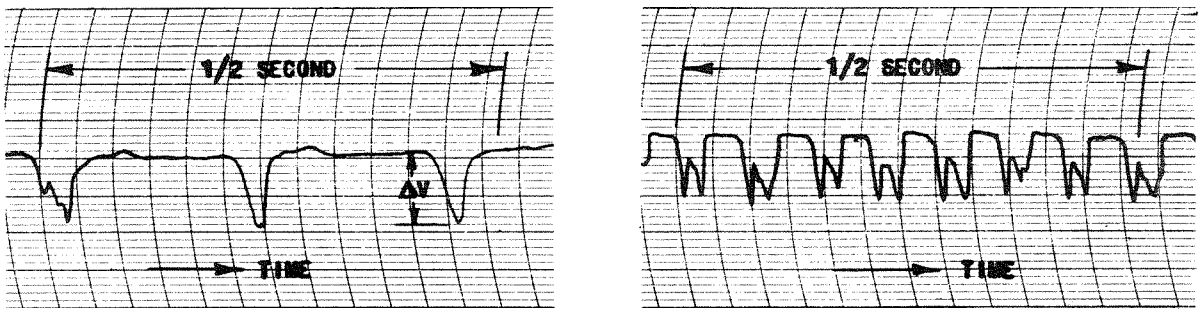

ONE-REGION PARTIAL STALL, $\bar{\Phi} = 0.39$
$R/R_0 = 0.65$, $\omega_s = 0.38\omega$, FAST CHART SPEED

THREE-REGION PARTIAL STALL, $\bar{\Phi} = 0.34$
$R/R_0 = 0.65$, $\omega_s = 0.38\omega$, FAST CHART SPEED

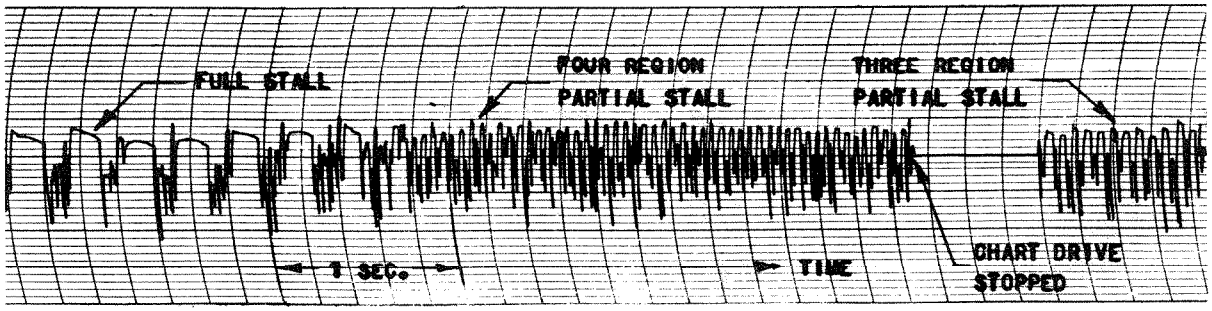

EXAMPLE OF UNSTABLE STALL PATTERN AT TRANSITION POINT. THROTTLE SETTING UNTOUCHED. CHANGE FROM FULL STALL TO THREE-REGION PARTIAL STALL WITH INTERMEDIATE FOUR-REGION PARTIAL STALL PATTERN. OPENING THROTTLE, $\bar{\Phi} = 0.339$, $R/R_0 = 0.611$, CONSTANT RPM.

FIGURE 14: OSCILLOGRAPH RECORDS OF PROPAGATING STALL. THREE-STAGE FREE VORTEX BLADING, BEHIND THIRD ROTOR ROW, 750 RPM

FIGURE 15
RADIAL VARIATION OF PEAK VELOCITY FLUCTUATION AMPLITUDE RATIOS
THREE-STAGE FREE VORTEX BLADING, 750 RPM
BEHIND THIRD ROTOR ROW

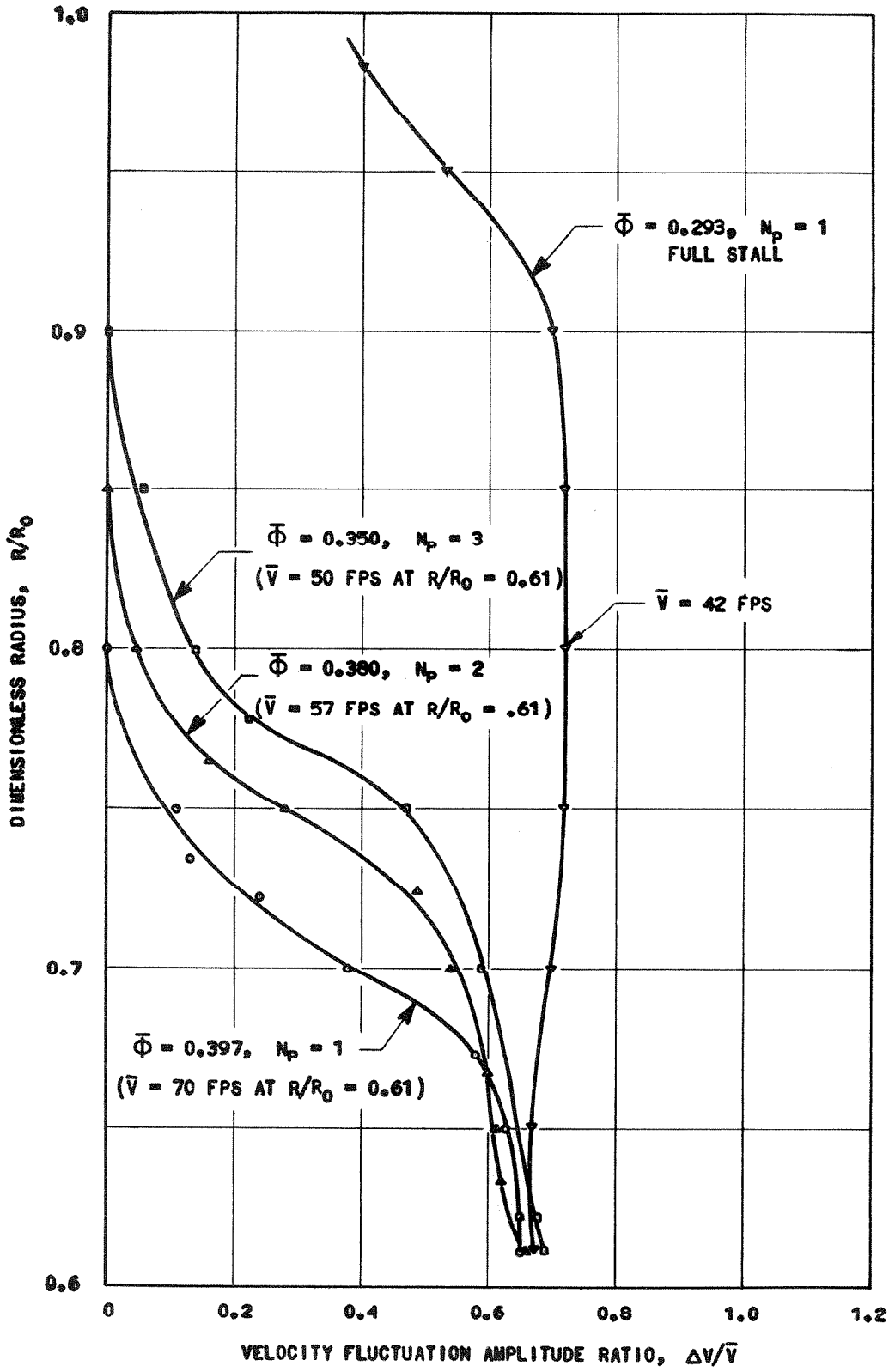

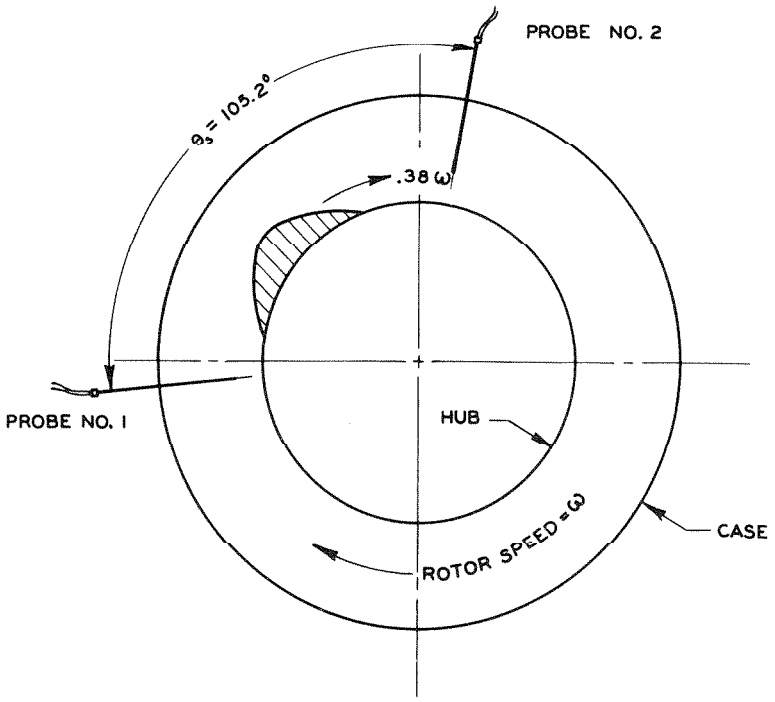

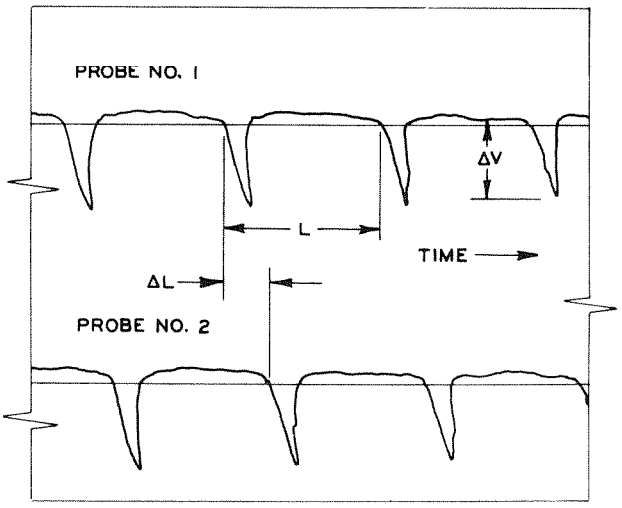

PHASE DATA

3 STAGE FREE VORTEX

BEHIND 3RD ROTOR

$R/R_o = 0.65$

$\bar{\Phi} = 0.40 \quad \omega_s = 0.38\omega$

θ_p = PHASE ANGLE

$= \frac{\Delta L}{L} \times 360° = 104°$

NO. OF REGIONS = $\frac{\theta_p}{\theta_s} \approx 1$

Fig. 16: Illustration of Phase Measurements for the Determination of the Number of Stalled Regions

FIGURE 17

RESULTS OF PHASE MEASUREMENTS FOR THE DETERMINATION OF STALL DISTURBANCE NUMBER

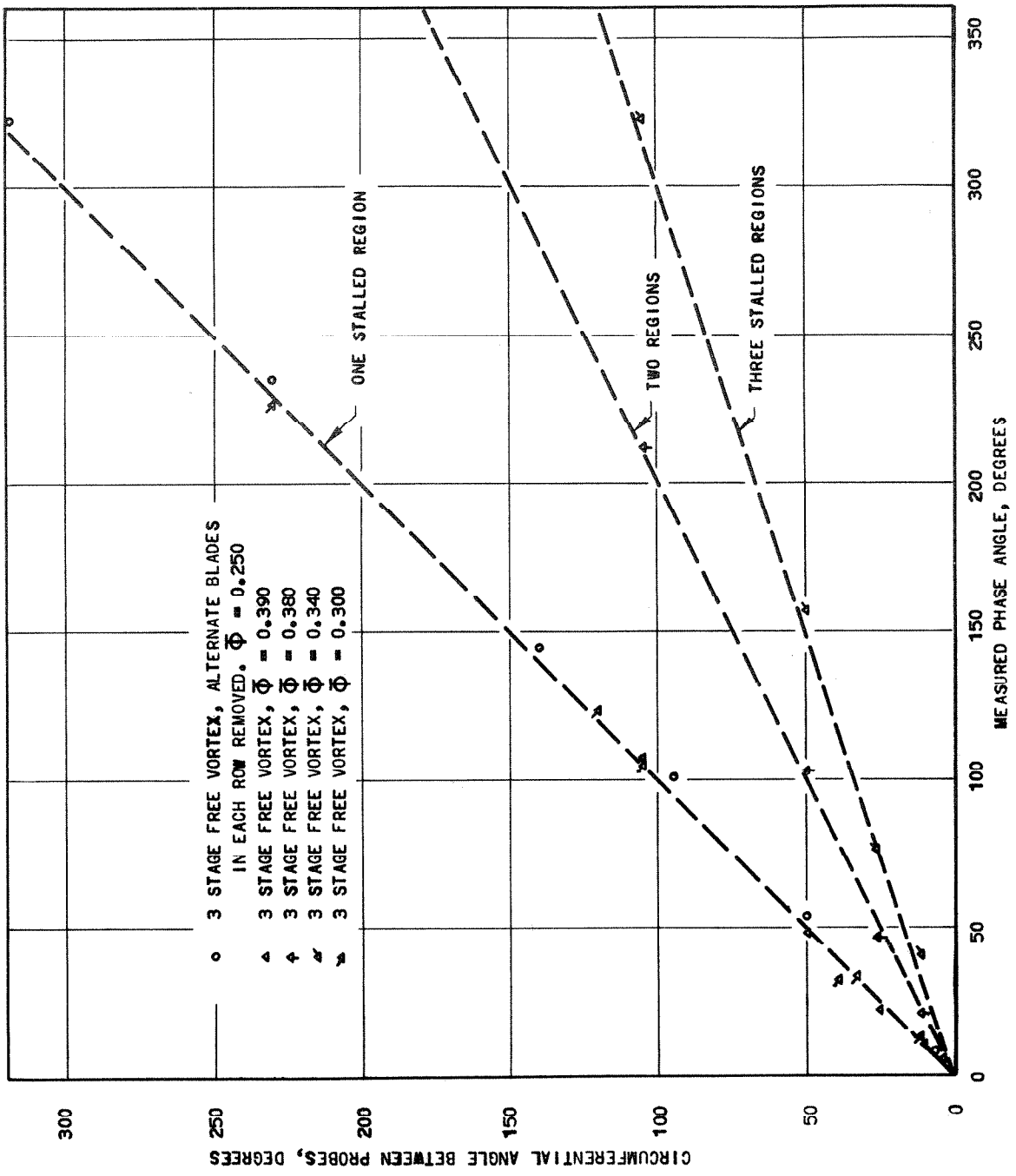

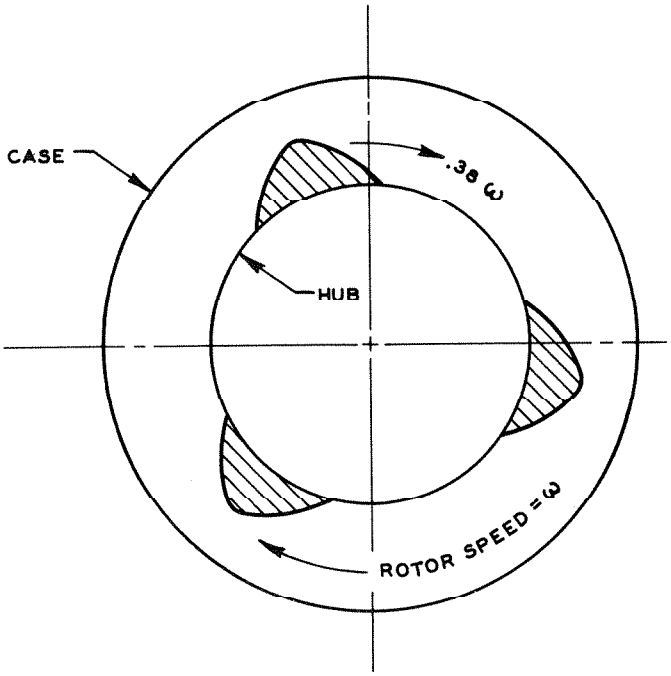

Fig. 18: Depiction of Three-Region Propagating Stall Pattern. Three-Stage Free Vortex Blading, $\bar{\Phi} = 0.363$ Behind Third Rotor Row, 750 rpm.

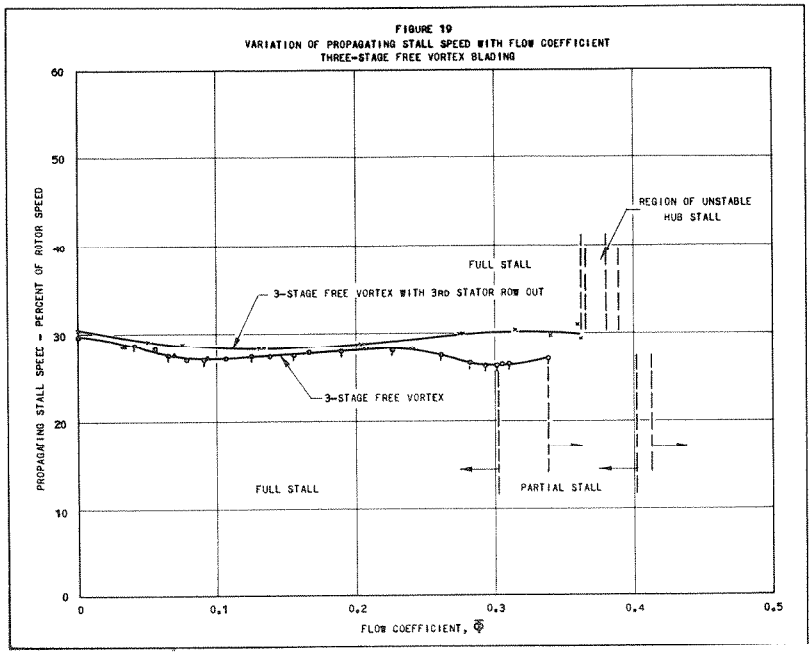

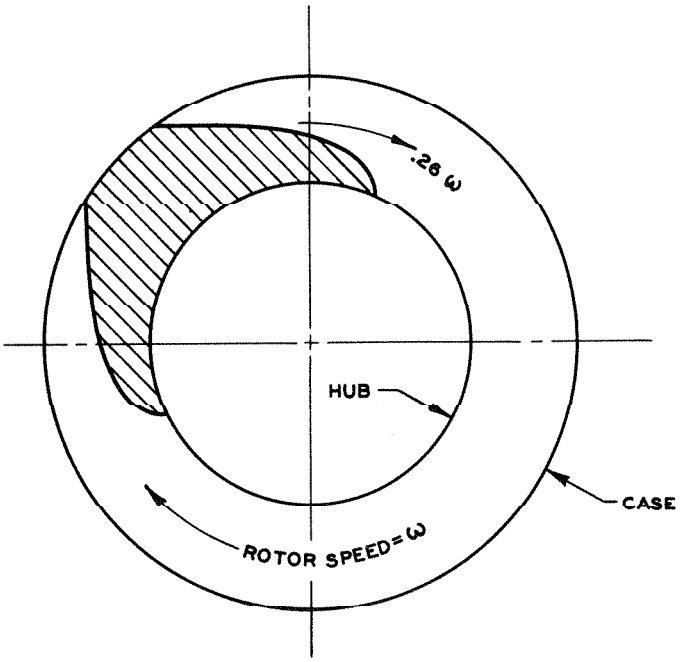

Fig. 20: Depiction of Full Stall Pattern (Looking into Compressor) $\bar{\Phi} = 0.323$ (opening throttle), Three-Stage Free Vortex Blading, Behind Third Rotor Row, 750 rpm

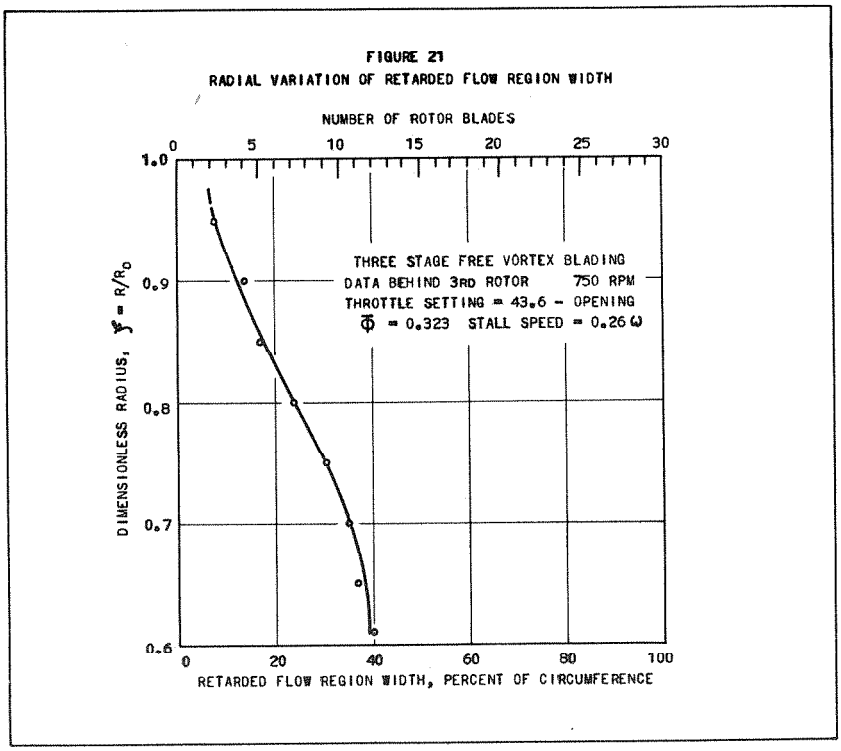

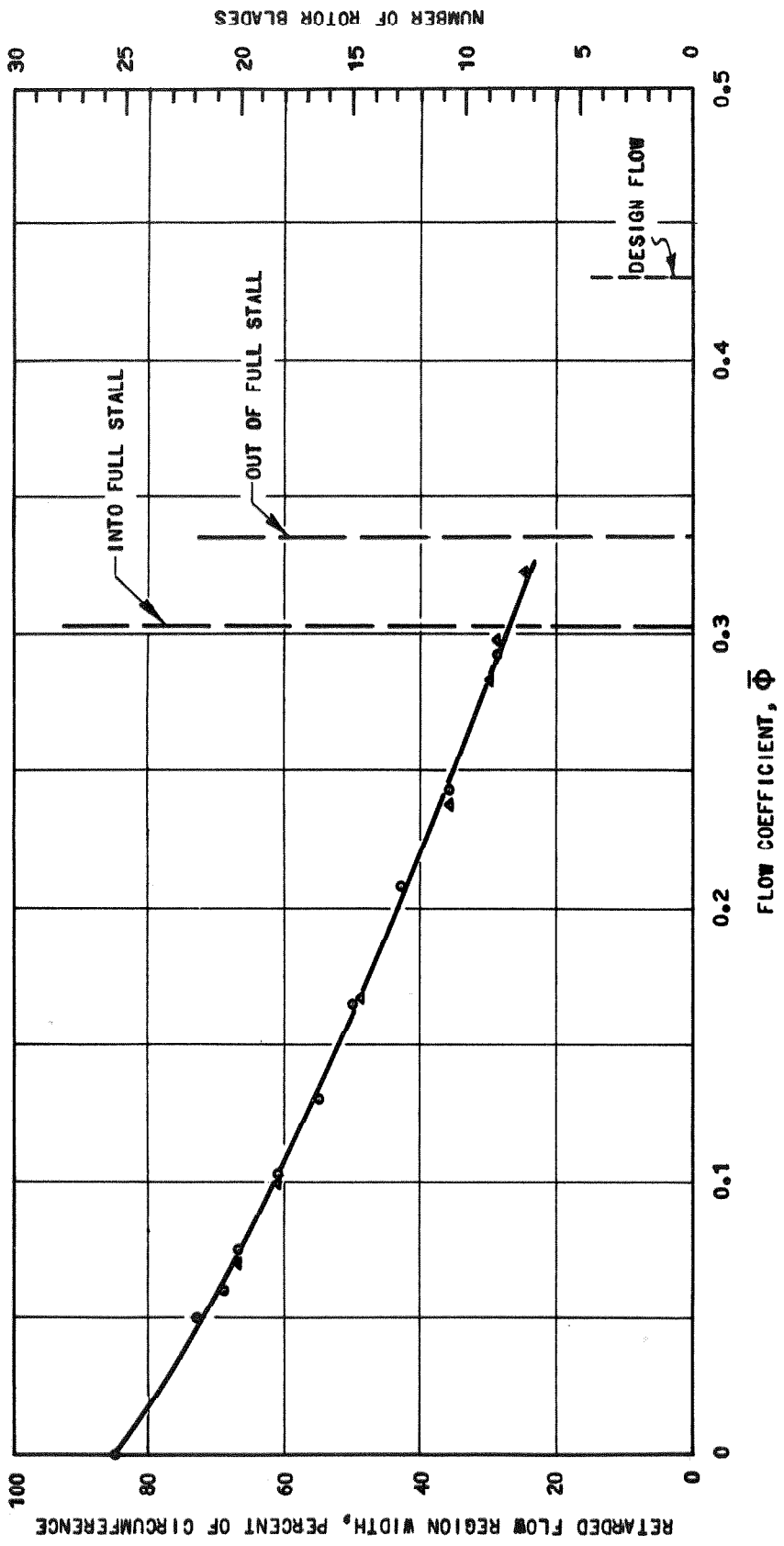

FIGURE 22
VARIATION OF RETARDED FLOW REGION WIDTH WITH FLOW COEFFICIENT
THREE-STAGE FREE VORTEX BLADING
DATA BEHIND THIRD ROTOR AT MID-BLADE HEIGHT, 750 RPM - FULL STALL

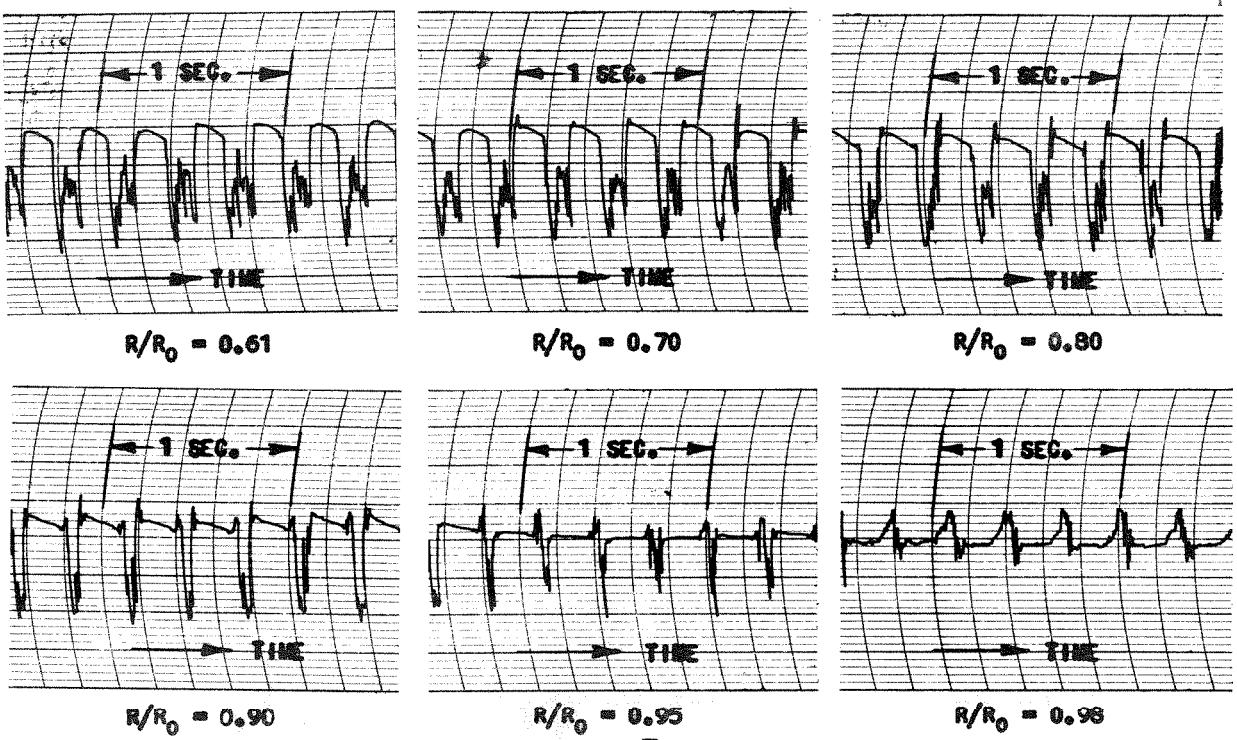

VELOCITY FLUCTUATIONS AT VARIOUS RADII, $\bar{\Phi} = 0.282$, BEHIND THIRD ROTOR ROW.
PROPAGATING STALL SPEED = 26 PERCENT OF ROTOR SPEED.

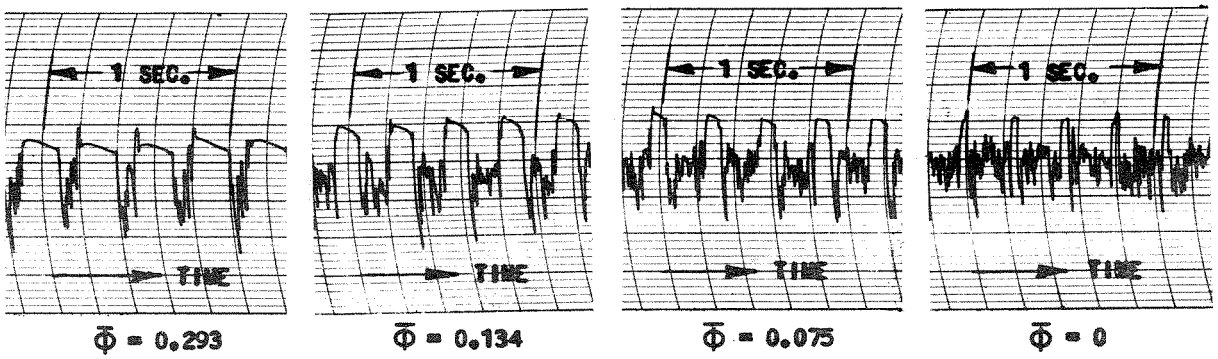

MID-BLADE HEIGHT VELOCITY FLUCTUATIONS AT VARIOUS FLOW COEFFICIENTS
DATA TAKEN BEHIND THIRD ROTOR ROW

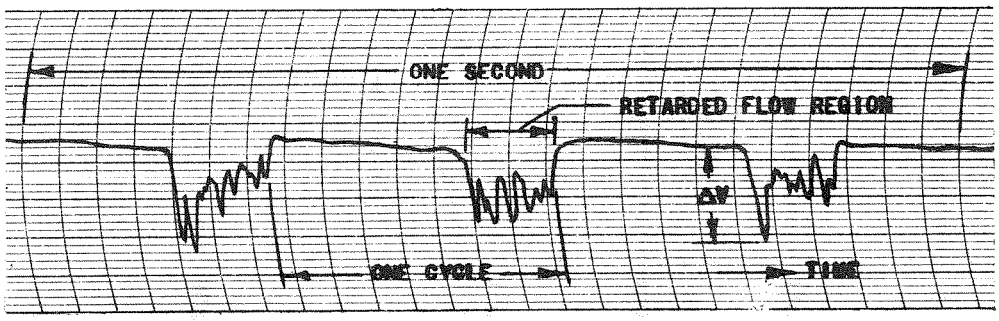

$\bar{\Phi} = 0.29$, BEHIND SECOND ROTOR ROW AT MID-BLADE HEIGHT, FAST CHART SPEED
PROPAGATING STALL SPEED = 26 PERCENT OF ROTOR SPEED

FIGURE 23: OSCILLOGRAPH RECORDS OF FULL STALL VELOCITY FLUCTUATIONS. THREE-STAGE FREE VORTEX BLADING, 750 RPM.

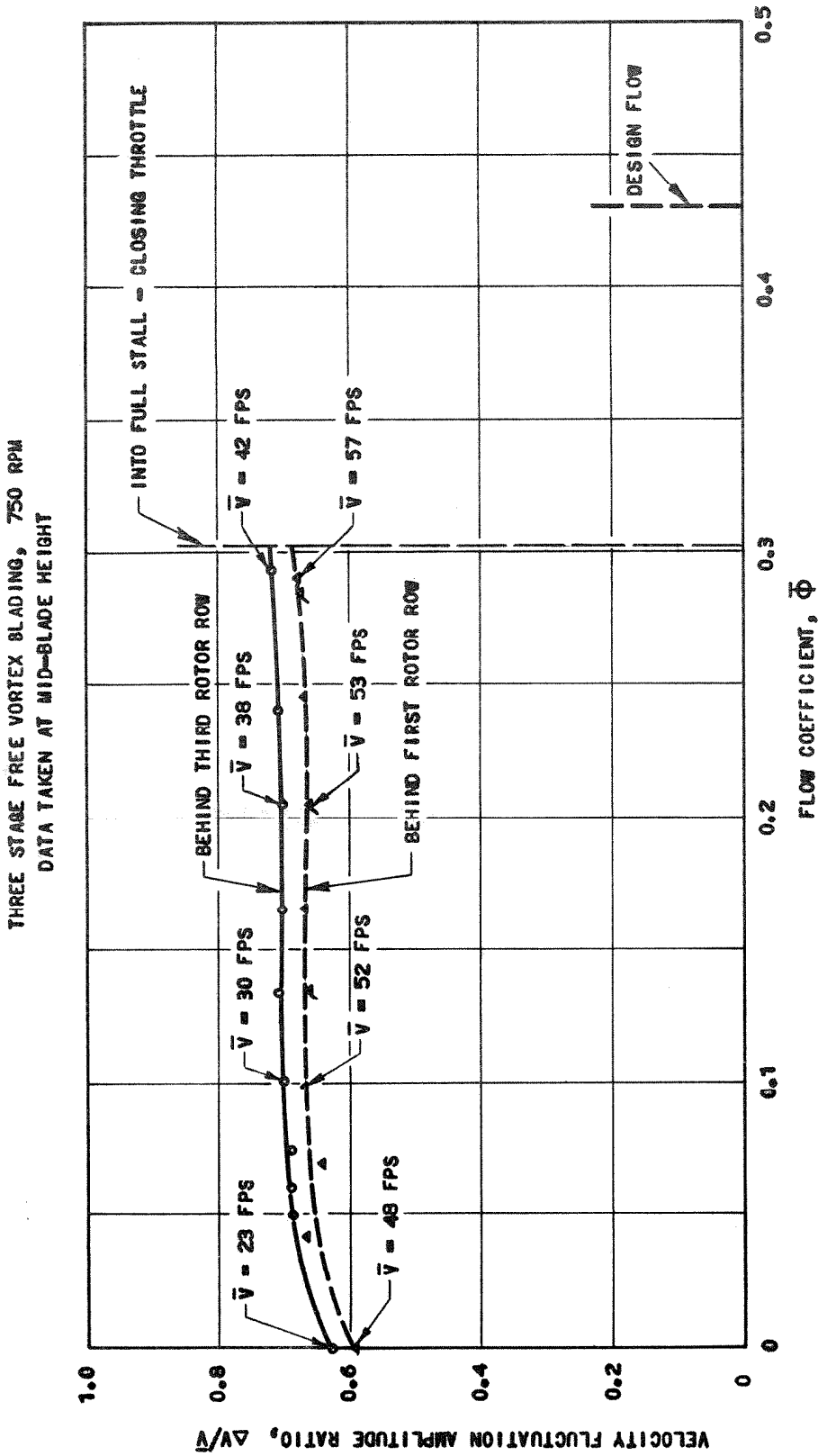

FIGURE 24
THREE STAGE FREE VORTEX BLADING, 750 RPM
DATA TAKEN AT MID-BLADE HEIGHT

FIGURE 25
VARIATION OF PROPAGATING STALL SPEED WITH FLOW COEFFICIENT
THREE-STAGE FREE VORTEX BLADING, 750 RPM
(ONE-HALF NORMAL COMPLEMENT OF BLADES)
BEHIND THIRD ROTOR

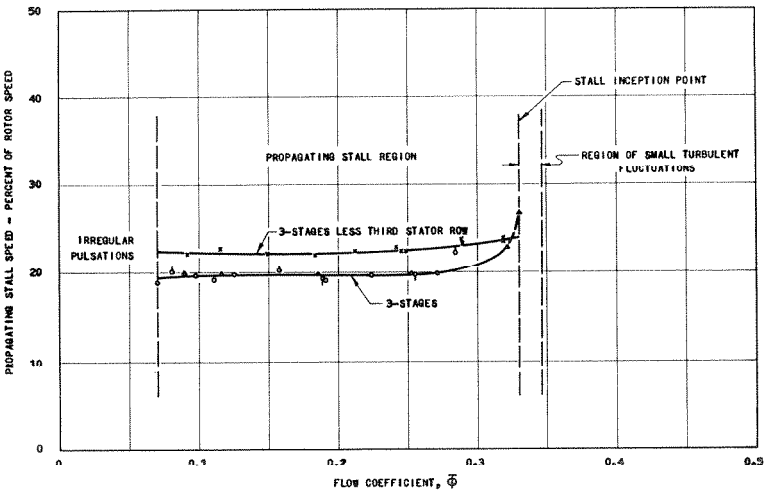

FIGURE 26
EFFECT OF SOLIDITY CHANGE ON PROPAGATING STALL SPEED AT $\bar{\Phi} = 0.20$
THREE-STAGE FREE VORTEX BLADING

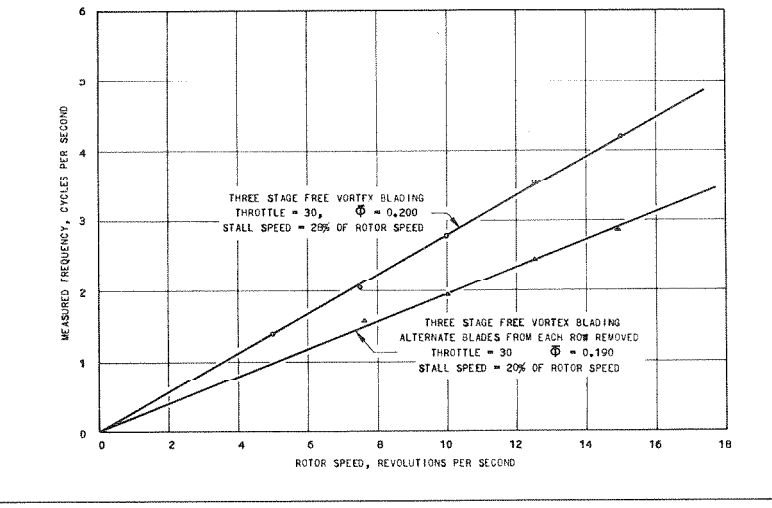

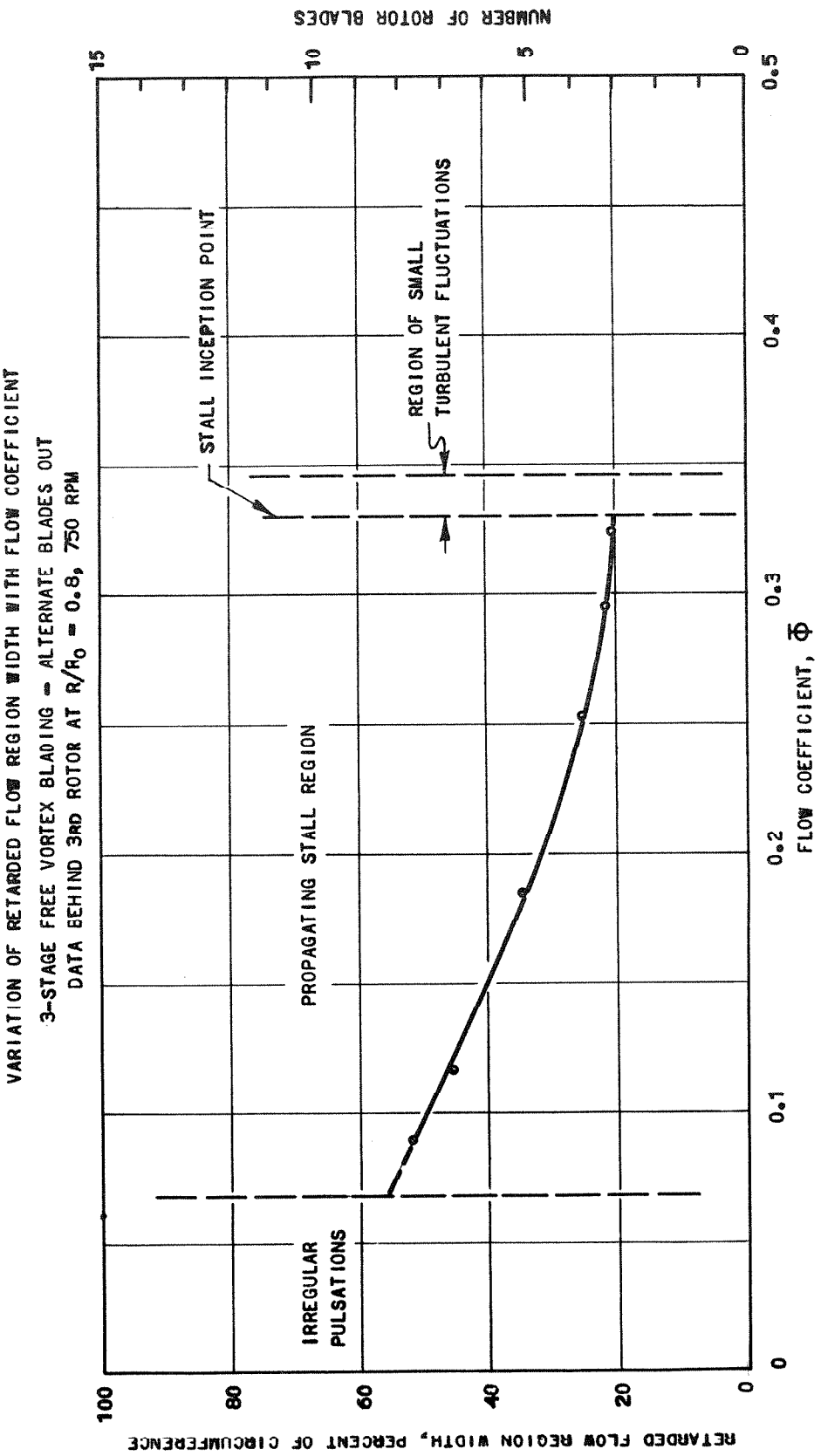

FIGURE 27
VARIATION OF RETARDED FLOW REGION WIDTH WITH FLOW COEFFICIENT
3-STAGE FREE VORTEX BLADING - ALTERNATE BLADES OUT
DATA BEHIND 3RD ROTOR AT $R/R_0 = 0.8$, 750 RPM

FIGURE 28
RADIAL VARIATION OF RETARDED FLOW REGION WIDTH
THREE-STAGE FREE VORTEX BLADING - 750 RPM
ONE-HALF NORMAL COMPLEMENT OF BLADES
BEHIND THIRD ROTOR

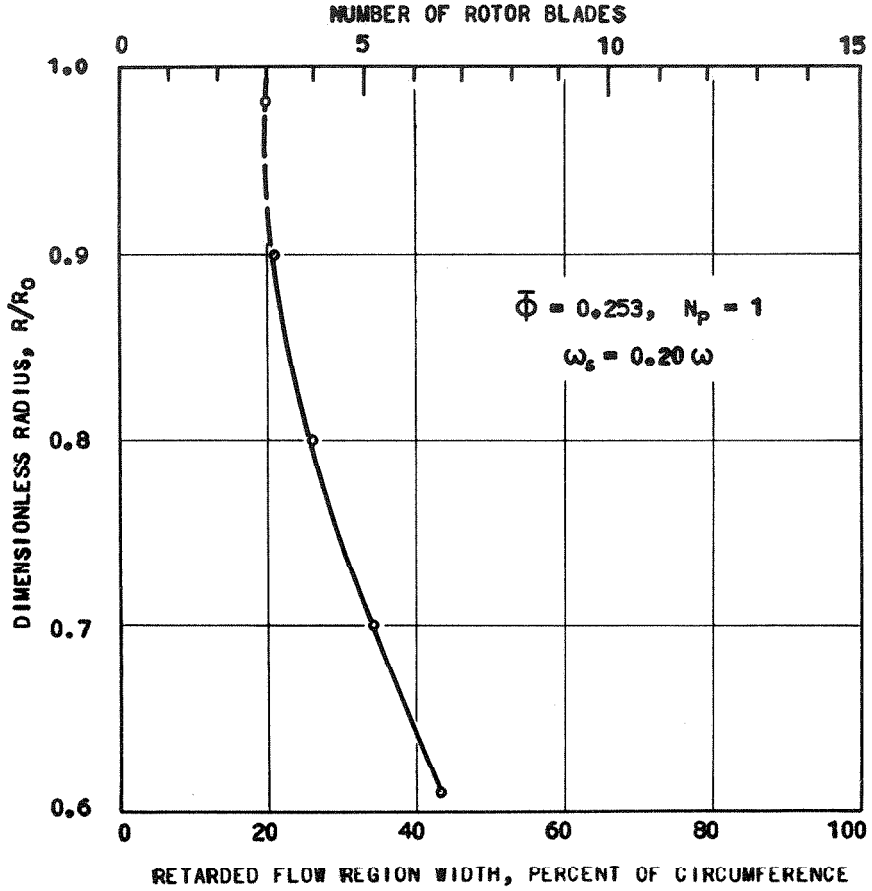

FIGURE 29
VARIATION OF EXIT-DUCT WALL PRESSURE WITH FLOW COEFFICIENT
ONE-STAGE FREE VORTEX BLADING - 750 RPM

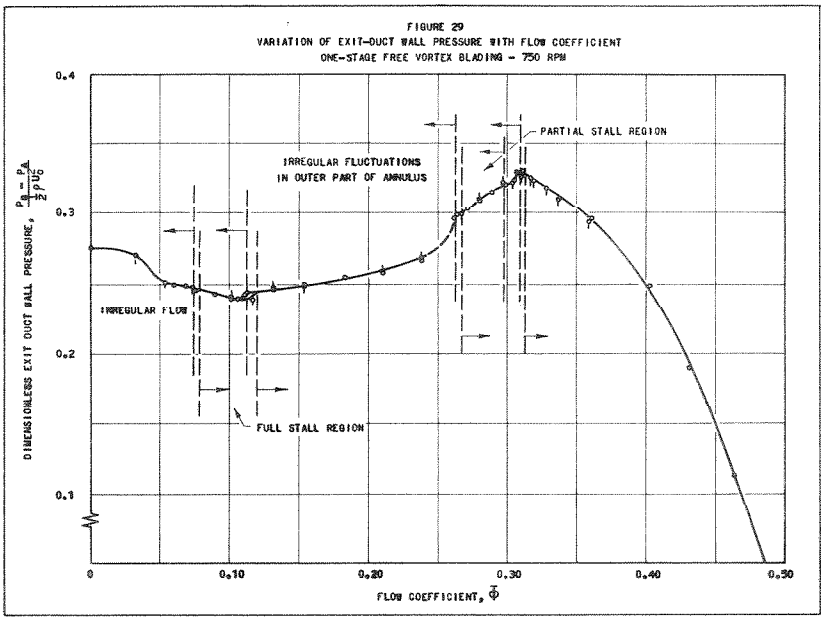

FIGURE 30
VARIATION OF PROPAGATING STALL SPEED WITH FLOW COEFFICIENT
ONE-STAGE FREE VORTEX BLADING - 750 RPM

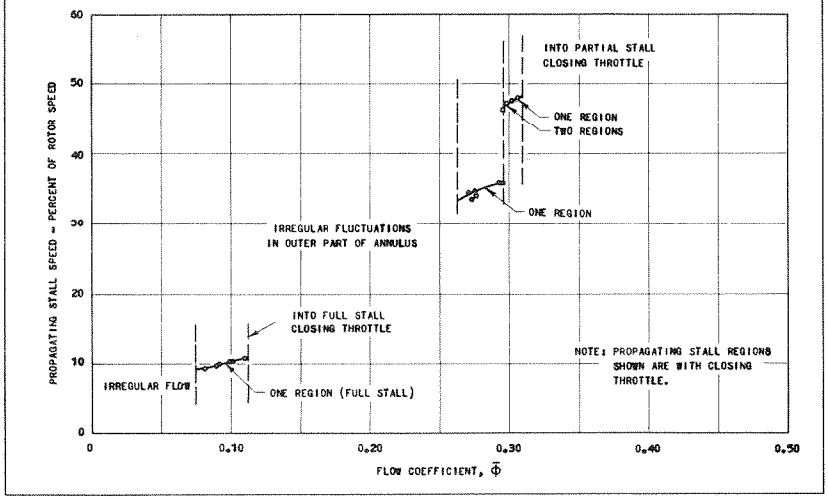

FIGURE 31

RESULTS OF PHASE MEASUREMENTS FOR THE DETERMINATION OF STALL DISTURBANCE NUMBER

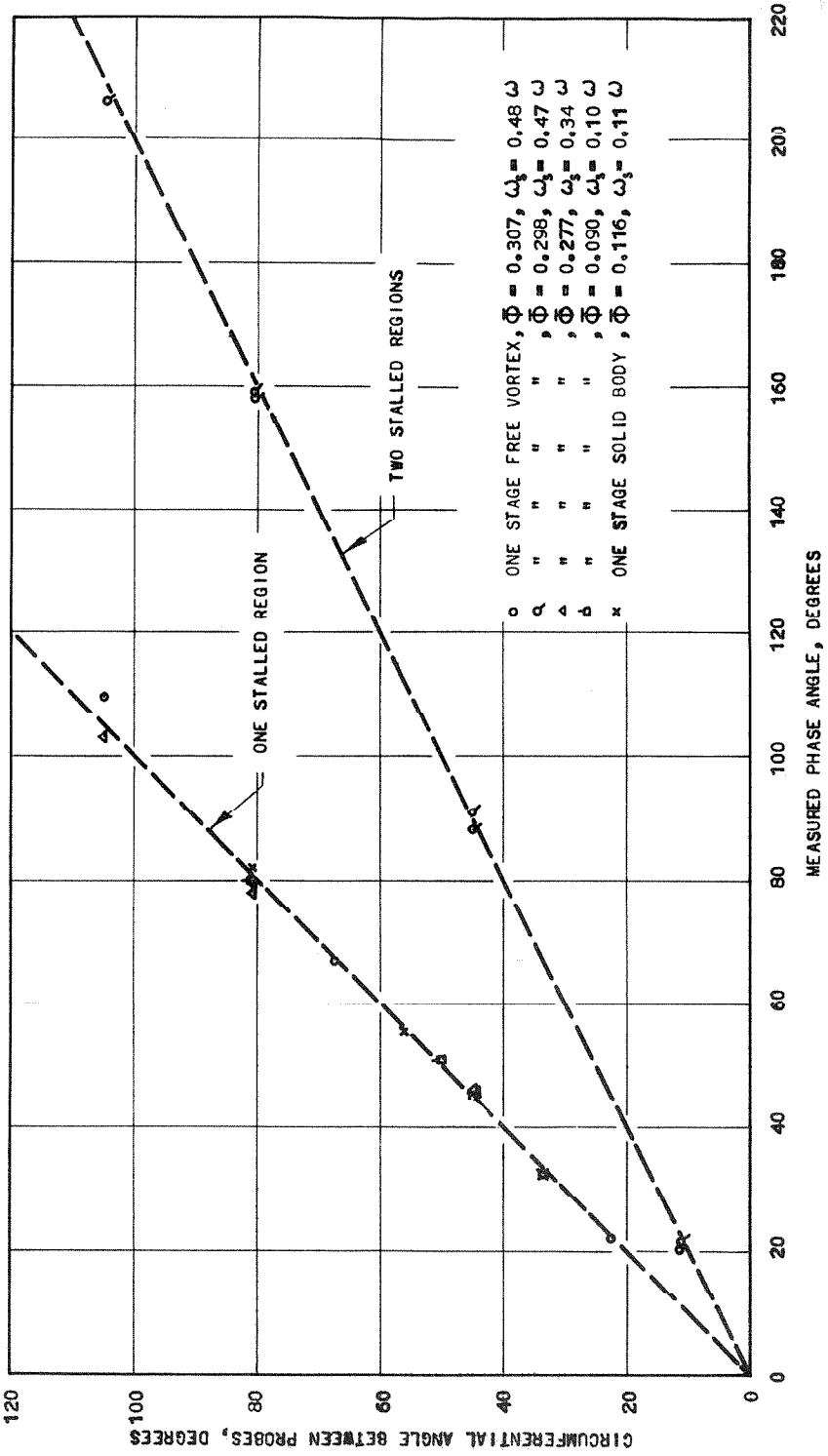

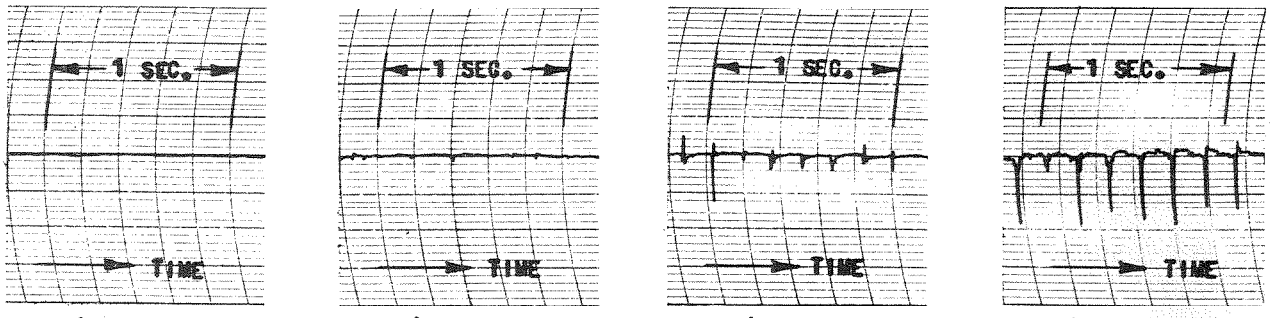

$R/R_0 = 0.70$ $R/R_0 = 0.80$ $R/R_0 = 0.90$ $R/R_0 = 0.98$

ONE-REGION PARTIAL STALL, $\bar{\Phi} = 0.307$ CLOSING THROTTLE, $\omega_s = 0.48\omega$

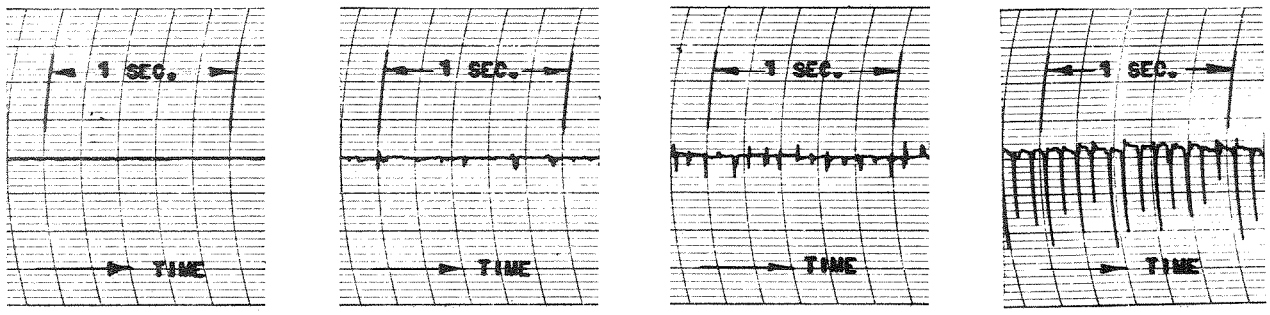

$R/R_0 = 0.65$ $R/R_0 = 0.80$ $R/R_0 = 0.90$ $R/R_0 = 0.98$

TWO-REGION PARTIAL STALL, $\bar{\Phi} = 0.300$ CLOSING THROTTLE, $\omega_s = 0.48\omega$

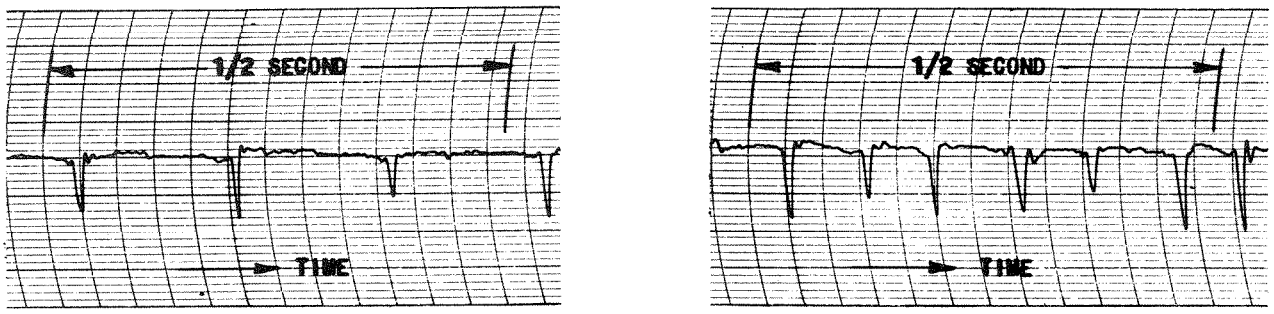

ONE-REGION PARTIAL STALL, $\bar{\Phi} = 0.307$
$R/R_0 = 0.98$, $\omega_s \cong 0.48\omega$, FAST CHART SPEED

TWO-REGION PARTIAL STALL, $\bar{\Phi} = 0.300$
$R/R_0 = 0.98$, $\omega_s \cong 0.48\omega$, FAST CHART SPEED

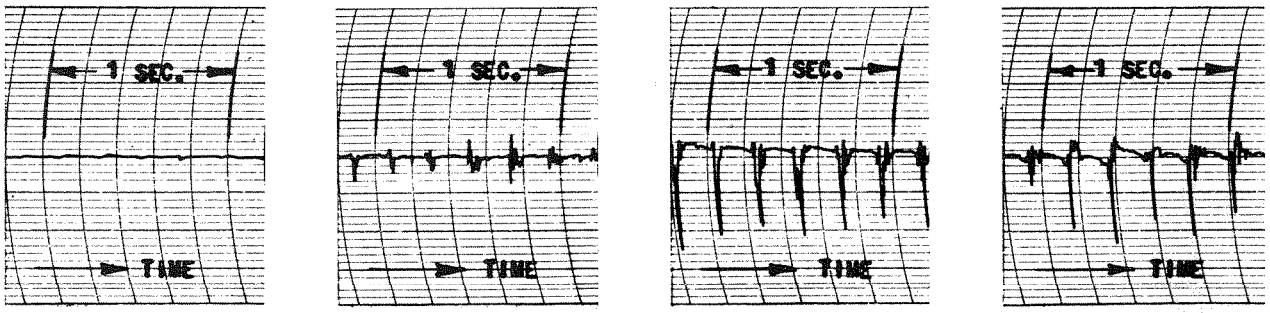

$R/R_0 = 0.61$ $R/R_0 = 0.80$ $R/R_0 = 0.90$ $R/R_0 = 0.98$

ONE-REGION PARTIAL STALL, $\bar{\Phi} = 0.298$ CLOSING THROTTLE, $\omega_s = 0.36\omega$

FIGURE 32: OSCILLOGRAPH RECORDS OF PARTIAL STALL VELOCITY FLUCTUATIONS. DATA BEHIND ROTOR, ONE-STAGE FREE VORTEX BLADING, 750 RPM.

FIGURE 33
RADIAL VARIATION OF VELOCITY FLUCTUATION AMPLITUDE RATIO
ONE STAGE FREE VORTEX BLADING, 750 RPM
BEHIND ROTOR

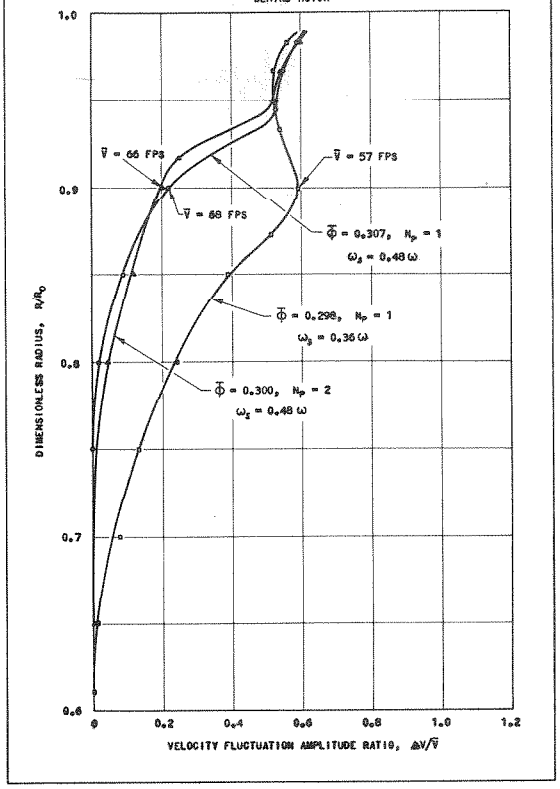

FIGURE 34
RADIAL VARIATION OF VELOCITY FLUCTUATION AMPLITUDE RATIO
ONE STAGE FREE VORTEX BLADING, 750 RPM
BEHIND ROTOR

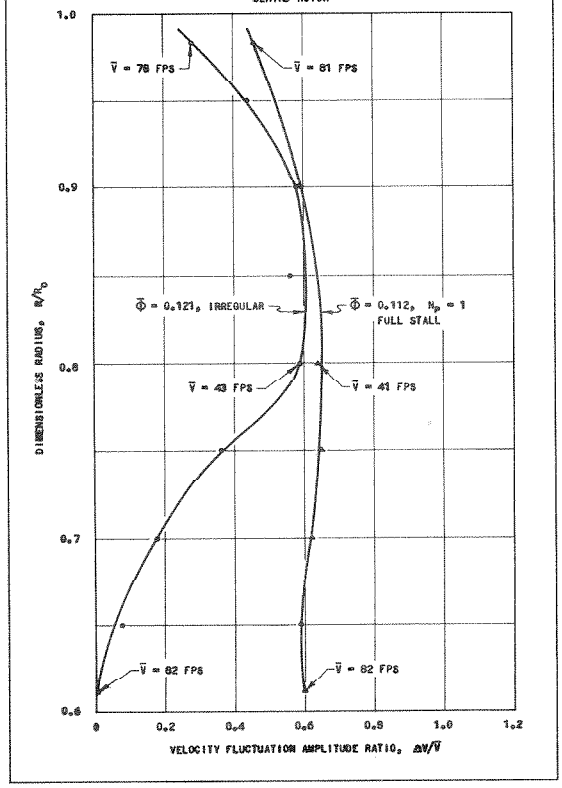

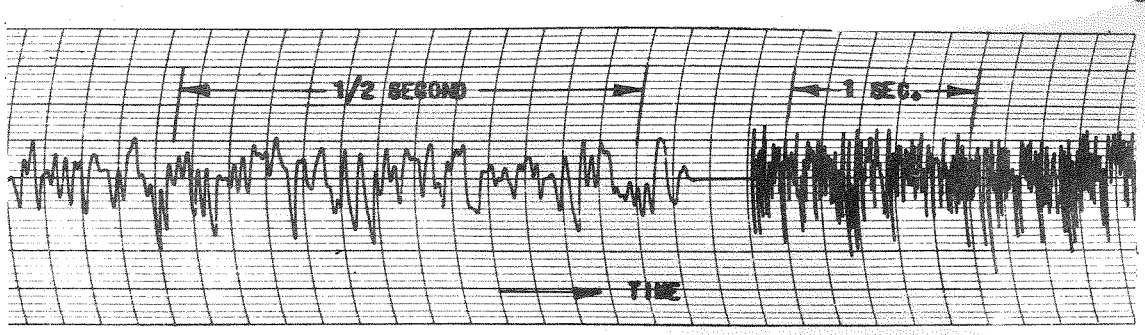

IRREGULAR VELOCITY FLUCTUATIONS IN OUTER PART OF ANNULUS. $\bar{\phi} = 0.160$ CLOSING THROTTLE
$R/R_0 = 0.950$, CHART SPEEDS OF 125 MM/SEC. AND 25 MM/SEC.

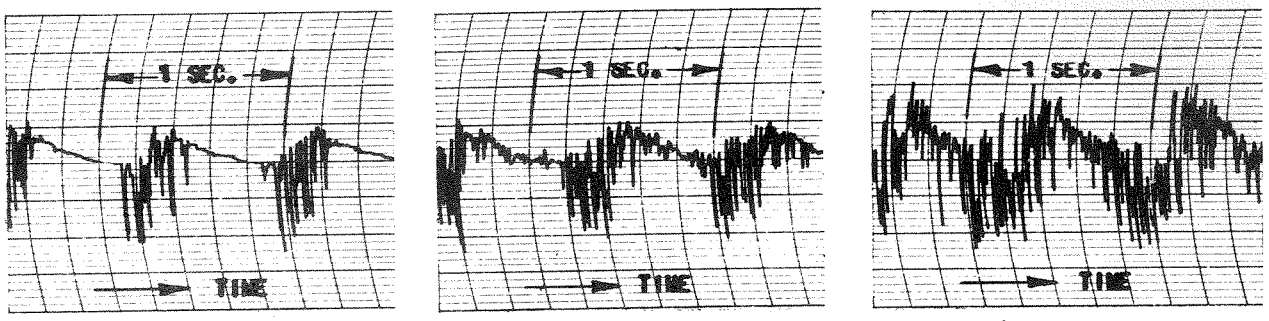

$R/R_0 = 0.61$ $R/R_0 = 0.70$ $R/R_0 = 0.80$

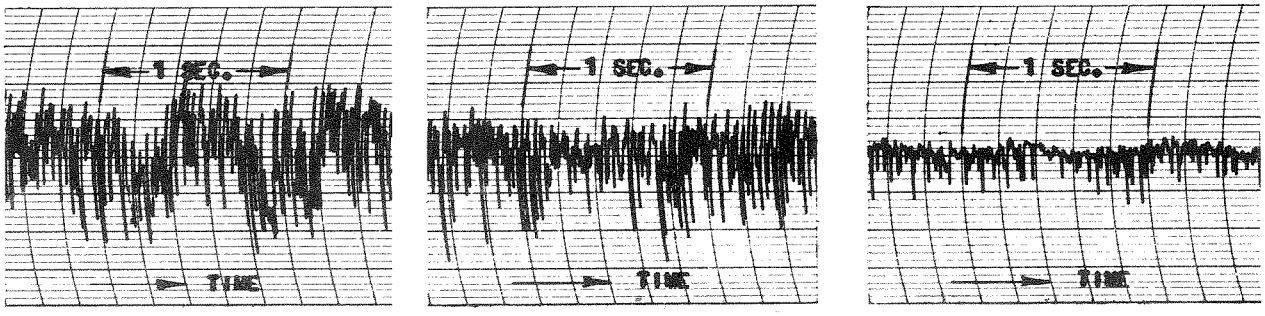

$R/R_0 = 0.90$ $R/R_0 = 0.95$ $R/R_0 = 0.98$

FULL STALL VELOCITY FLUCTUATIONS AT VARIOUS RADII. $\bar{\phi} = 0.090$ CLOSING THROTTLE
PROPAGATING STALL SPEED = 10 PERCENT OF ROTOR SPEED

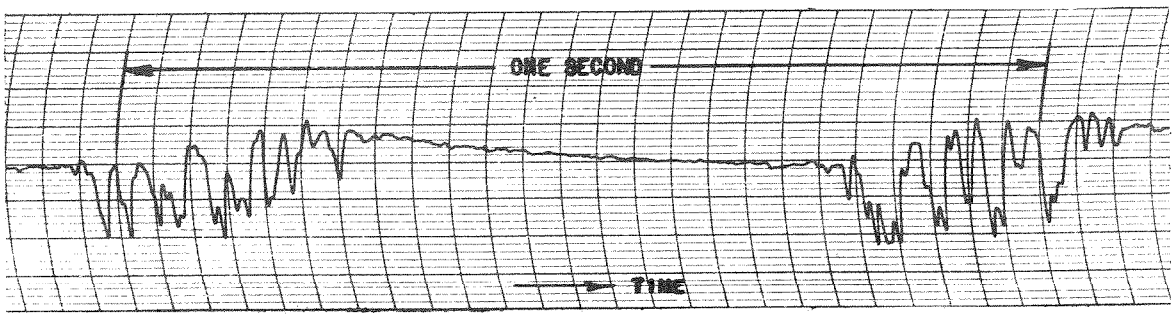

FULL STALL VELOCITY FLUCTUATIONS $\bar{\phi} = 0.090$, $R/R_0 = 0.61$, $\omega_s = 0.10\omega$
FAST CHART SPEED (125 MM/SEC.)

FIGURE 35: OSCILLOGRAPH RECORDS OF VELOCITY FLUCTUATIONS. ONE-STAGE FREE VORTEX BLADING DATA BEHIND ROTOR ROW, 750 RPM.

FIGURE 36
RADIAL VARIATION OF RETARDED FLOW REGION WIDTH

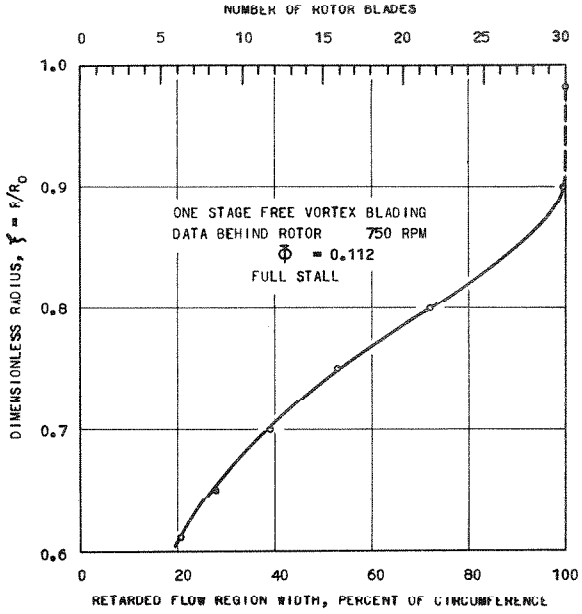

FIGURE 37
VARIATION OF RETARDED FLOW REGION WIDTH WITH FLOW COEFFICIENT
ONE-STAGE FREE VORTEX BLADING - 750 RPM
BEHIND ROTOR AT R/R_0 = 0.611

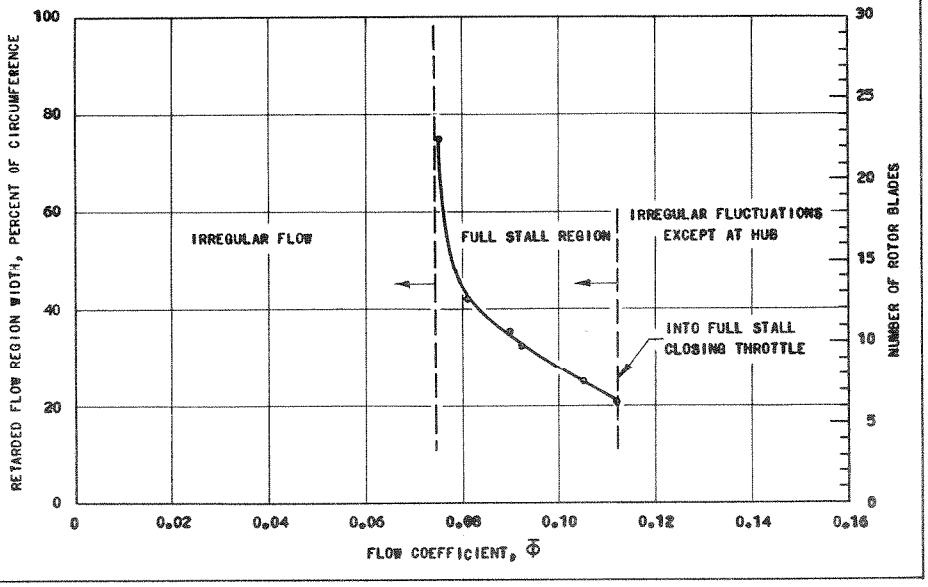

FIGURE 38
VARIATION OF EXIT-DUCT WALL PRESSURE WITH FLOW COEFFICIENT
ONE-STAGE SOLID BODY BLADING - 750 RPM

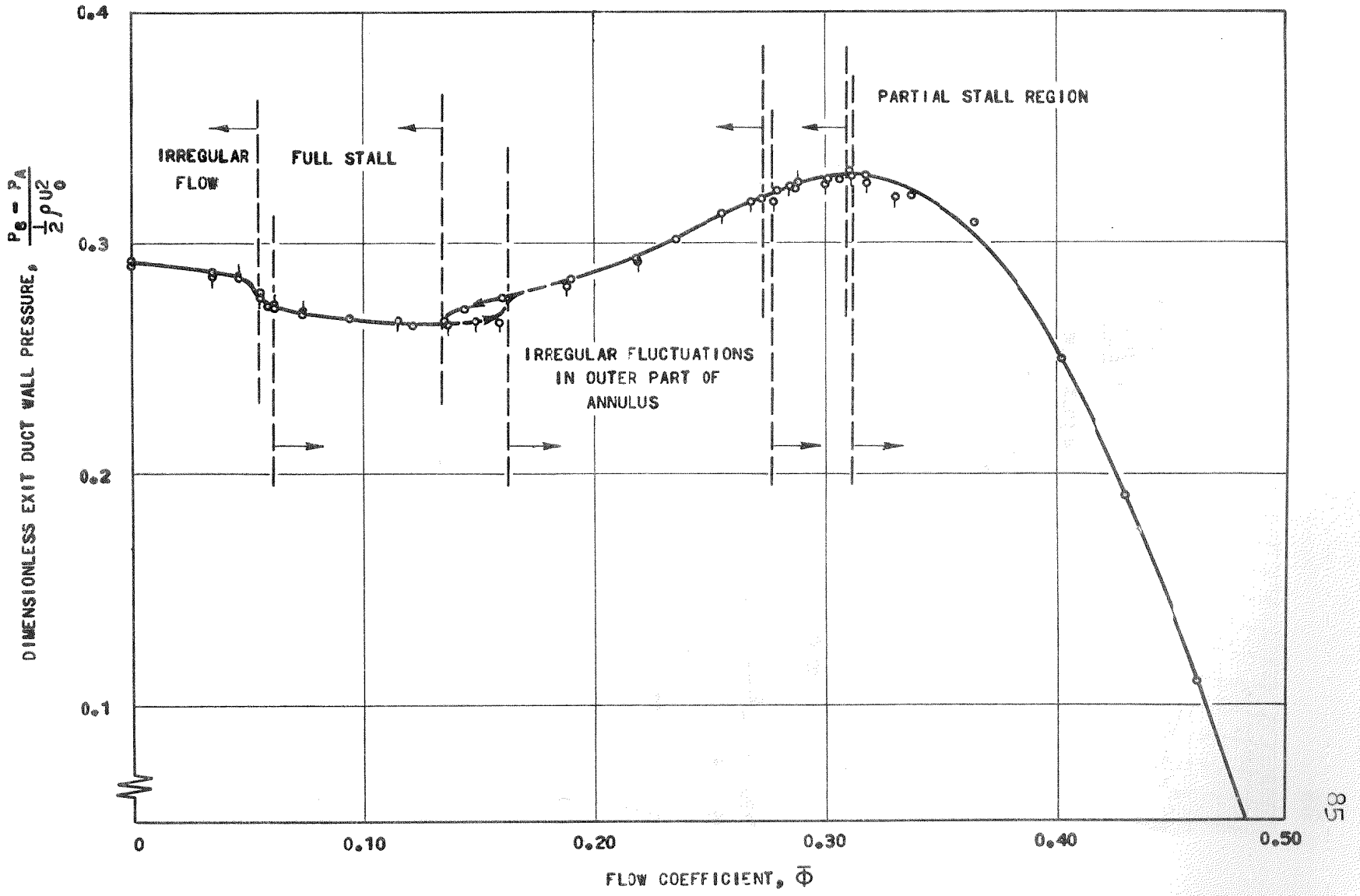

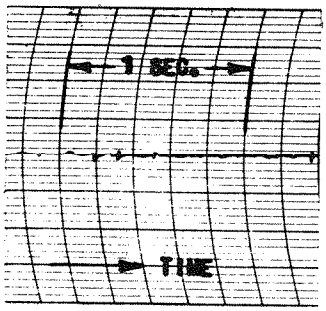

$R/R_0 = 0.80$

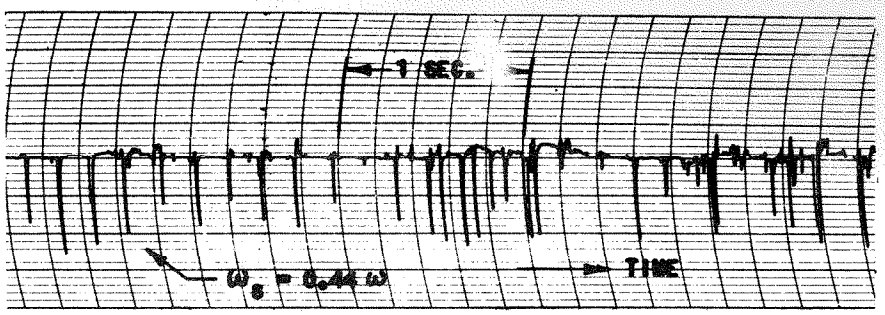

$R/R_0 = 0.983$

ONE-REGION PARTIAL STALL (UNSTABLE), $\bar{\Phi} = 0.308$ CLOSING THROTTLE, INITIAL STALL POINT.

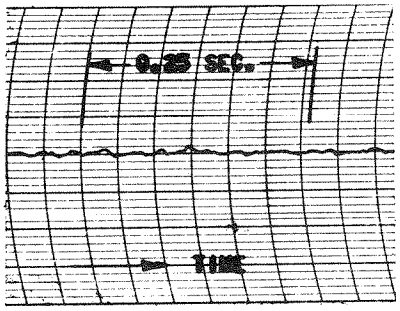

$R/R_0 = 0.611$

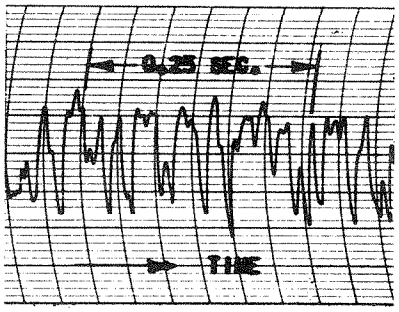

$R/R_0 = 0.800$

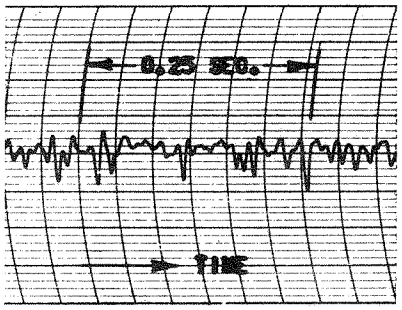

$R/R_0 = 0.983$

IRREGULAR VELOCITY FLUCTUATIONS, LARGELY IN OUTER PART OF ANNULUS, $\bar{\Phi} = 0.139$ CLOSING THROTTLE
FAST CHART SPEED (125 MM/SEC.)

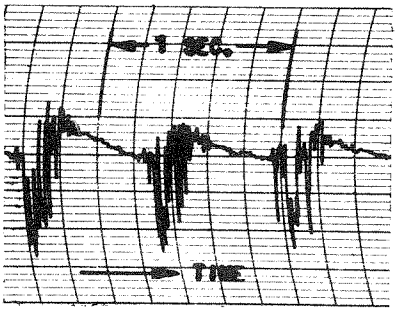

$R/R_0 = 0.700$

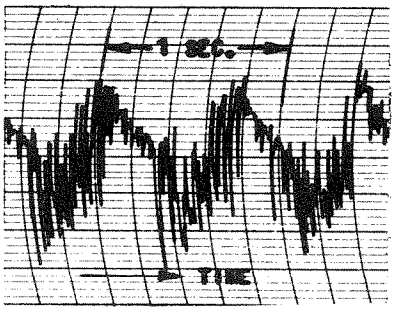

$R/R_0 = 0.800$

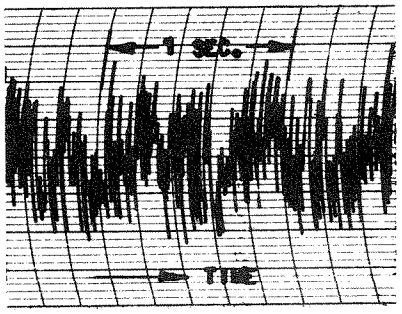

$R/R_0 = 0.900$

FULL STALL VELOCITY FLUCTUATIONS AT VARIOUS RADII. $\bar{\Phi} = 0.129$ CLOSING THROTTLE, $\omega_s = 0.11\,\omega$
(INTERMEDIATE CHART SPEED - 25 MM/SEC.)

FIGURE 39: OSCILLOGRAPH RECORDS OF VELOCITY FLUCTUATIONS.
ONE-STAGE SOLID BODY BLADING, BEHIND ROTOR,
750 RPM.

FIGURE 40
RADIAL VARIATION OF VELOCITY FLUCTUATION AMPLITUDE RATIO
ONE STAGE SOLID BODY BLADING, 750 RPM
BEHIND ROTOR

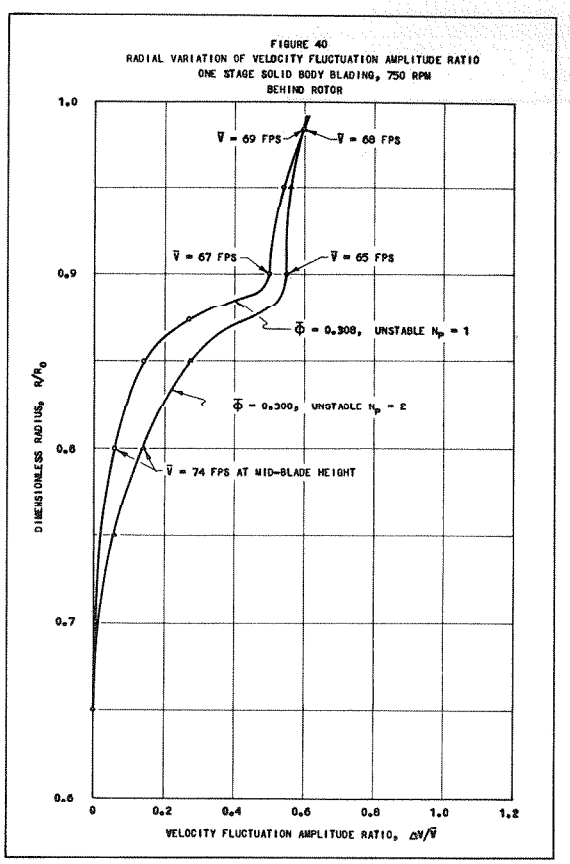

FIGURE 41
RADIAL VARIATION OF VELOCITY FLUCTUATION AMPLITUDE RATIO
ONE STAGE SOLID BODY BLADING, 750 RPM
BEHIND ROTOR

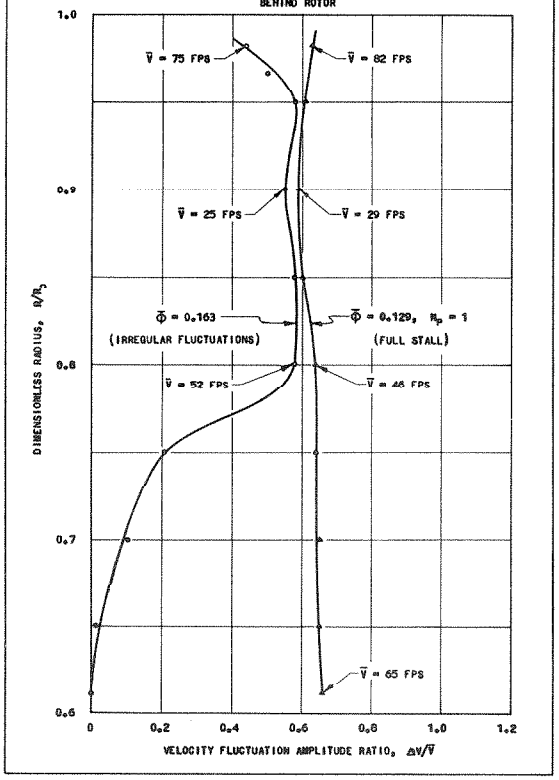

FIGURE 42
VARIATION OF FULL STALL PROPAGATING STALL SPEED WITH FLOW COEFFICIENT
ONE-STAGE SOLID BODY BLADING - 750 RPM
DATA BEHIND ROTOR

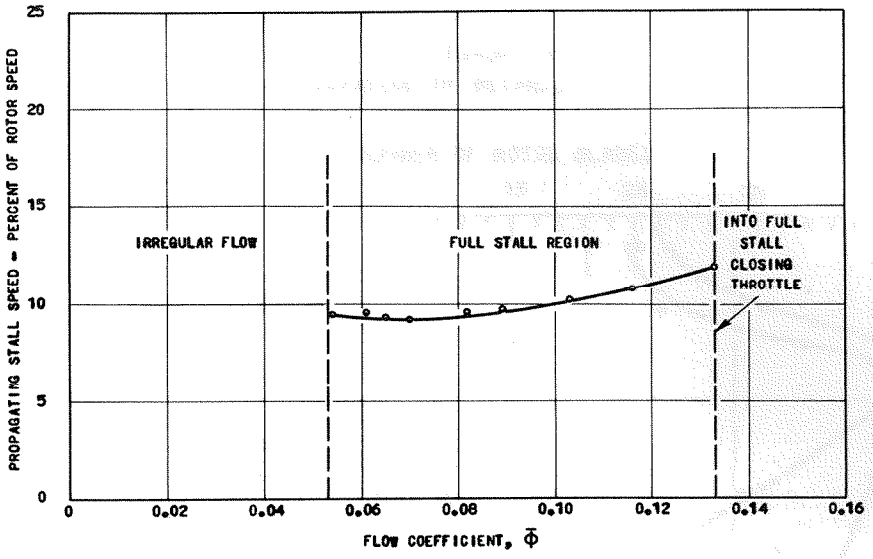

FIGURE 43
VARIATION OF RETARDED FLOW REGION WIDTH WITH FLOW COEFFICIENT
ONE-STAGE SOLID BODY BLADING - 750 RPM
BEHIND ROTOR AT $R/R_0 = 0.611$

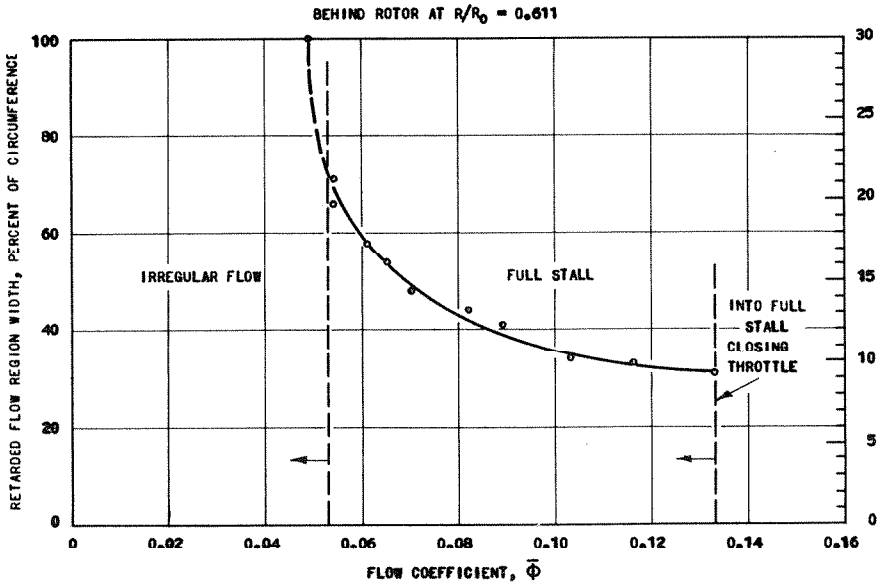

FIGURE 44
RADIAL VARIATION OF RETARDED FLOW REGION WIDTH